

# Mineralogical and geochemical characteristics of the host-rocks from Ag-polymetallic Rupice deposit, Bosnia and Herzegovina

---

Vokić, Ema

Master's thesis / Diplomski rad

2024

Degree Grantor / Ustanova koja je dodijelila akademski / stručni stupanj: **University of Zagreb, Faculty of Mining, Geology and Petroleum Engineering / Sveučilište u Zagrebu, Rudarsko-geološko-naftni fakultet**

Permanent link / Trajna poveznica: <https://urn.nsk.hr/urn:nbn:hr:169:921938>

Rights / Prava: [In copyright](#) / [Zaštićeno autorskim pravom](#).

Download date / Datum preuzimanja: **2025-03-25**



Repository / Repozitorij:

[Faculty of Mining, Geology and Petroleum Engineering Repository, University of Zagreb](#)



UNIVERSITY OF ZAGREB  
FACULTY OF MINING, GEOLOGY AND PETROLEUM ENGINEERING  
Graduate study of Geology

**MASTER'S THESIS**

Mineralogical and geochemical characteristics of the host-rocks from Ag-  
polymetallic Rupice deposit, Bosnia and Herzegovina

Ema Vokić

G-2174

Zagreb, 2024.



Sveučilište u Zagrebu  
RUDARSTVO-GEOLOŠKO-NAFTNI FAKULTET  
HR-10000 Zagreb, Prilježeva 6, t.p. 300

OBRAZAC SUSTAVA UPRAVLJANJA KVALITETOM

KLASA: 602-01/24-01/22  
URBROJ: 251-70-13-242  
U Zagrebu, 15.02.2024.

**Emma Vokić, studentica**


## RJEŠENJE O ODOBRENJU TEME

Na temelju vašeg zahtjeva primljenog pod KLASOM 602-01/24-01/22, URBROJ: 251-70-13-241 od 02.02.2024. priopćujemo vam temu diplomskog rada koja glasi:

**Mineralogical and geochemical characteristics of the host-rocks from Ag-polymetallic Rupice deposit, Bosnia and Herzegovina**

Za mentoricu ovog diplomskog rada imenuje se u smislu Pravilnika o izradi i obrani diplomskog rada Prof.dr.sc. Sibila Borojević Šošćarić nastavnik Rudarsko-geološko-naftnog-fakulteta Sveučilišta u Zagrebu.

Mentorica:

  
(potpis)

Prof.dr.sc. Sibila Borojević  
Šošćarić

(titula, ime i prezime)

Predsjednica povjerenstva za  
završne i diplomske ispite:

  
(potpis)

Izv.prof.dr.sc. Ana Maričić

(titula, ime i prezime)

Prodekan za nastavu i studente

  
(potpis)

Izv.prof.dr.sc. Borivoje  
Pašić

(titula, ime i prezime)

Oznaka: OB 8.5.-1 SRF-1-13/0

Stranica: 1/1

Čuvanje (godina) Trajno

## ACKNOWLEDGMENTS

*I want to express my gratitude to my mentor, Dr. sc. Sibila Borojević Šoštarić, for her trust, encouragement, readiness to help, kind words, and the knowledge I have gained through the years of our collaboration.*

*I am deeply thankful to Dr. sc. Duje Smirčić for sharing his sedimentological knowledge, and to Dr. sc. Duje Kukoč and Dr. sc. Tonči Grgasović for their paleontological expertise.*

*Special thanks to Dr. Sc. Tomislav Brenko for conducting the XRD analysis and interpreting the results.*

*Thanks to our technician, Mario Valent, for preparing the samples.*

*I sincerely thank geologists Sergei Smolonogov, Theodore Veligrakis, and Marko Matic from company Adriatic Metals, who generously shared their knowledge and assisted me. I have learned a lot from you.*

*Special thanks to my dear family and friends, who listened to my doubts and thoughts about the work, supported me during this academic journey and gave me the strength to see this through.*

MINERALOGICAL AND GEOCHEMICAL CHARACTERISTICS OF THE HOST-ROCKS  
FROM AG-POLYMETALLIC RUPICE DEPOSIT, BOSNIA AND HERZEGOVINA

Ema Vokić

Thesis completed at: University of Zagreb  
Faculty of Mining, Geology and Petroleum Engineering  
Department of Mineralogy, Petrology and Mineral Resources  
Pierottijeva 6, 10 000 Zagreb

Abstract

The Triassic succession of the Rupice deposit comprises deep-sea siliciclastic-carbonate, volcanoclastic, and chert units. Five cores were selected for petrographic and geochemical analysis to determine the characteristics and deposition conditions of lithotypes, as well as the genesis of the deposit. Five facies and eleven lithotypes were differentiated: 1. Siliciclastic-carbonate facies (lithotypes dolomitic marl, silicified marl, dolomitic siltstone, silicified siltstone, dolomicrite, LD dolomite, and dolomite breccia), 2. Spilite facies (lithotypes tuff, amygdaloidal basalt, spilite breccia), 3. Chert facies (lithotype radiolarite), 4. Ore-bearing facies (sulphide mineralization and mineralized dolomitic breccia), and 5. Limestone facies (lithotype mudstone). The deep-sea siliciclastic-carbonate facies were deposited in the Anisian during the opening of the Dinaric Tethys, followed by advanced rifting in the Anisian-Ladinian, which was accompanied by the deposition of radiolarite and followed by a magmatic-hydrothermal phase. In the Eocene-Oligocene, the basin closure occurred through reverse faulting, resulting in overthrusts and a duplex structure of the deposit.

Keywords: Ag-polymetallic Rupice deposit, duplex structure, Dinaric Tethys sedimentation basin

Master's thesis includes: 60 pages, 19 tables, 26 figures, and 21 references.

Original in: English

Archived at: Library of the Faculty of Mining, Geology and Petroleum Engineering, Pierottijeva 6, Zagreb

Supervisors: Prof. Sibila Borojević Šoštarić, PhD  
Tech. assistance: Senior Assistant Tomislav Brenko, PhD  
Reviewers: Prof. Sibila Borojević Šoštarić, PhD  
Assist. Prof. Duje Smirčić, PhD  
Assoc. Prof. Stanko Ružičić, PhD

Defense date: February 22<sup>nd</sup>, 2024, Faculty of Mining, Geology and Petroleum Engineering, University of Zagreb

## TABLE OF CONTENTS

<b>1.</b>	<b>INTRODUCTION.....</b>	<b>1</b>
<b>2.</b>	<b>GEOGRAPHICAL SETTING.....</b>	<b>2</b>
<b>3.</b>	<b>GEOLOGICAL SETTING .....</b>	<b>3</b>
<b>3.1.</b>	<b>Regional geological setting.....</b>	<b>3</b>
<b>3.2.</b>	<b>Local geological setting .....</b>	<b>6</b>
<b>4.</b>	<b>SAMPLING AND ANALYTICAL METHODS .....</b>	<b>10</b>
<b>4.1.</b>	<b>Polarized light microscopy.....</b>	<b>11</b>
<b>4.2.</b>	<b>Colouring of the carbonates.....</b>	<b>11</b>
<b>4.3.</b>	<b>X-ray diffraction analysis .....</b>	<b>12</b>
<b>4.4.</b>	<b>X-ray fluorescence analysis.....</b>	<b>12</b>
<b>4.5.</b>	<b>Fossils age determination .....</b>	<b>13</b>
<b>5.</b>	<b>RESULTS.....</b>	<b>14</b>
<b>5.1.</b>	<b>Field study .....</b>	<b>14</b>
5.1.1.	Siliciclastic – carbonate facies .....	16
5.1.2.	Spilite facies.....	18
5.1.3.	Chert facies.....	19
5.1.4.	Ore – bearing facies (the Main and the Upper mineralization zone) .....	19
5.1.5.	Dolomitic breccia facies.....	20
5.1.6.	Limestone facies.....	20
<b>5.2.</b>	<b>Polarized light microscopy.....</b>	<b>21</b>
5.2.1.	Siliciclastic-carbonate facies.....	22
5.2.2.	Spilite facies.....	29
5.2.3.	Chert facies .....	33
5.2.4.	Ore – bearing facies .....	34
5.2.5.	Dolomite breccia facies.....	36
5.2.6.	Limestone facies.....	37
5.2.7.	Contact zones .....	38
<b>5.3.</b>	<b>X-ray diffraction analysis.....</b>	<b>39</b>
<b>5.4.</b>	<b>X-ray fluorescence analysis .....</b>	<b>41</b>
5.4.1.	Major elements.....	41
5.4.2.	Trace elements .....	42
<b>5.5.</b>	<b>Fossils age determination .....</b>	<b>43</b>
5.5.1.	Radiolarian dating.....	43
5.5.2.	Foraminifera dating.....	45
<b>6.</b>	<b>DISCUSSION .....</b>	<b>45</b>

<b>6.1. Interpretation of depositional conditions and environment of facies</b> .....	45
6.1.1. Footwall host rocks – Siliciclastic-carbonate facies (LT1A, LT2A, LT3) .....	45
6.1.2. Hanging wall – radiolarite (LT7) .....	45
6.1.3. Magmatic-hydrothermal event.....	46
6.1.4. Limestone facies (LT11) .....	47
<b>6.2. Alterations</b> .....	48
6.2.1. Mechanism of dolomitization .....	48
6.2.2. Spilite alterations.....	48
6.2.3. Silicification and sericitization.....	49
6.2.4. Framboidal pyrite .....	49
<b>6.3. Genesis of the Rupice deposit</b> .....	49
6.3.1. The first phase: Anisian.....	49
6.3.2. The second phase: Anisian – Ladinian.....	50
6.3.3. The third phase: Eocene – Oligocene.....	51
6.3.4. The fourth phase: recent.....	52
<b>7. CONCLUSION</b> .....	<b>53</b>
<b>8. REFERENCES</b> .....	<b>55</b>

## LIST OF FIGURES

<b>Figure 1-1.</b> Location of the Rupice concession.....	2
<b>Figure 2-1.</b> Geographical position of study area.....	3
<b>Figure 3-1.</b> Geological map of the Central Dinarides.....	6
<b>Figure 3-3.</b> Ore body model of the Rupice deposit.....	9
.....	11
<b>Figure 4-1.</b> Red spots indicate the position of the petrographic thin section within drill-cores.....	11
<b>Figure 5-1.</b> Lithological units of the MOB. ....	15
<b>Figure 5-2.</b> Lithological units of the NW ore body.....	16
<b>Figure 5-3.</b> The position of the samples <b>A)</b> MOB-BR-49-19-11, <b>B)</b> NW-29-22-04, <b>C)</b> MOB-BRD-27-22-15, <b>D)</b> MOB-BR-49-19-20, <b>E)</b> NW-11-22-01, and <b>F)</b> NW-11-22-08 .....	18
<b>Figure 5-4.</b> The position of the sample <b>A)</b> MOB-BR-49-19-25, <b>B)</b> MOB-BR-49-19-18, <b>C)</b> MOB-BRD-27-22-27 .....	19
<b>Figure 5-5.</b> The position of the samples <b>A)</b> NW-29-22-01 and <b>B)</b> NW-21-22-03 .....	19
<b>Figure 5-6.</b> The position of the sample MOB-BRD-27-22-24.....	20
<b>Figure 5-7.</b> The position of the sample NW-21-22-02.....	20
<b>Figure 5-8.</b> The position of the sample MOB-BRD-27-22-03.....	21
<b>Figure 5-9.</b> a) Classification and nomenclature of clastic sediments based on grain size; b) Classification of marls based on the proportion of siliciclastic and carbonate mud.....	21
<b>Figure 5-10.</b> Thin section micro-photographs of dolomitic marl.....	23
<b>Figure 5-11.</b> Thin section micro-photographs of silicified marl.....	24
<b>Figure 5-12.</b> Thin section micro-photographs of dolomitic siltstone.....	26
<b>Figure 5-13.</b> Thin section micro-photographs of sample NW-11-22-01 .....	27
<b>Figure 5-14.</b> Thin section micro-photographs of hypidiomorphic opaque ore minerals and the idiomorphic tabular and rozzete-like barite .....	36
<b>Figure 5-22.</b> Thin section micro-photographs of NW-21-22-02 sample .....	37
<b>Figure 5-15.</b> Thin section micro-photographs of tuff. ....	39
<b>Figure 5-16.</b> Middle Triassic radiolarians from sample NW21-22-03 .....	44
.....	44
<b>Figure 5-17.</b> Stratigraphic ranges of selected radiolarian species.....	44
<b>Figure 6-1.</b> Anisian opening of the Tethys basin. ....	50



**Figure 6-2.** A) Anisian-Ladinian advanced rifting, associated with spilite eruption on the seafloor; B) Ore-bearing hydrothermal event and alteration halos.....51

**Figure 6-3.** A) Eocene-Oligocene basin closure and reverse faulting; B) recent duplex-structure of the deposit.....52

## LIST OF TABLES

<b>Table 4-1.</b> List of chosen representative samples and conducted analyses.....	10
<b>Table 5-1.</b> Mineral composition of dolomitic marl.....	22
<b>Table 5-2.</b> Mineral composition of silicificated marl.....	23
<b>Table 5-3.</b> Mineral composition of dolomitic siltstone.....	25
<b>Table 5-4.</b> Mineral composition of silicificated siltstone.....	27
<b>Table 5-5.</b> Mineral composition of silty, clayey ED dolostone.....	27
<b>Table 5-6.</b> Mineral composition of silty, sandy LD dolomite.....	28
<b>Table 5-7.</b> Mineral composition of tuff.....	30
<b>Table 5-8.</b> Mineral composition of amygdaloidal basalt.....	31
<b>Table 5-9.</b> Mineral composition of spilite breccia.....	32
<b>Table 5-10.</b> Mineral composition of radiolarite.....	33
<b>Table 5-11.</b> Mineral composition of barite-sulphide mineralization.....	34
<b>Table 5-12.</b> Mineral composition of mineralized dolomite breccia.....	36
<b>Table 5-13.</b> Mineral composition of dolomite breccia.....	37
<b>Table 5-14.</b> Mineral composition of limestone.....	38
<b>Table 5-15.</b> XRD analysis results.....	40
<b>Table 5-16.</b> XRF analysis results (%). .....	42
<b>Table 5-17.</b> XRF analysis results (ppm).....	43
<b>Table 8-1.</b> Catalogue of the lithotypes.....	57

## LIST OF USED SYMBOLS AND UNITS

<b>Symbol</b>	<b>Description</b>
MOB	Main Ore Body
NW	Northwest Ore Body
LD Dol	Late-diagenetic dolomite
Brt	Barite
Cal	Calcite
Cel	Celadonite
Dol	Dolomite
Fe-Dol – Ank	Ferrous dolomite-ankerite
Pl	Plagioclase
Py	Pyrite
Qtz	Quartz

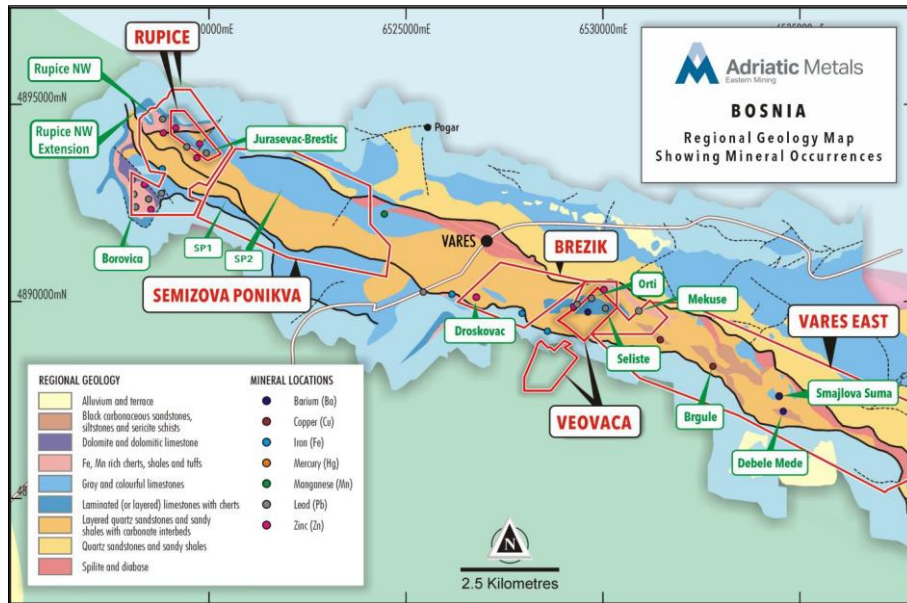
## 1. INTRODUCTION

As a part of the Vareš metallogenic province, the Rupice deposit is located 45 km north of Sarajevo in Central Bosnia and Herzegovina. In the early stages of Alpine orogenesis, the Vareš region was a part of the Tethyan sedimentary basin, where SW overthrusting of Triassic and Jurassic sediments formed stacked thrust nappes, contributing to the Dinaric orogeny. The Rupice deposit is located within the Durmidor nappe. The province, influenced by Triassic rifting magmatism, hosts various mineralization, including the Zn-Pb-BaSO<sub>4</sub> Veovača deposit, Pb-Zn Droškovac, and the Orti "Baritised breccia" with Pb-Zn sulphides.

Rupice hosts a 650m long massive sulphide mineralization, referred to as the Main Ore Body (MOB), true thicknesses up to 20m, and a separate ore body, Rupice Northwest (RNW), extending approximately 250m with open mineralization in various directions. The mineralization is formed in Triassic sediments, primarily within a brecciated dolomitic unit. Rupice's polymetallic mineralization includes 156 g/t Ag, 1.2 g/t Au, 4.3% Zn, 2.8% Pb, 0.4% Cu, 27% BaSO<sub>4</sub>, and a wide range of ore minerals, such as barite, galena, sphalerite, pyrite, chalcopyrite, and various sulfosalts (Adriatic Metals Plc, 2023).

Company Adriatic Metals Plc holds the exploration concession for the Rupice deposit, which is currently under exploration (Fig. 1-1.). The mineralogy and petrology of the lithological units of the deposit have not been thoroughly investigated yet, nor has the genetic model of the deposit. There are assumptions that the deposit is a hybrid of volcanogenic massive sulphide (VMS) and sedimentary-exhalative (SEDEX)-type ore genesis, but further drilling exploration is needed to determine the origin of the deposit more precisely.

This study aims to classify the lithological rock types within the deposit and their mineralogical, petrological, and geochemical characteristics and depositional conditions using micropetrographic, X-ray diffraction (XRD), and X-ray fluorescence (XRF) analysis. Furthermore, considering that the age of mineralization and surrounding rocks is presumed to be Middle Triassic, this study also focuses on determining the age using index fossils. Characteristics necessary for identifying lithotypes will be presented in a catalogue consisting of macroscopic and microscopic descriptions of individual units, their average mineral composition, depositional conditions, and specific ages. Moreover, based on all mentioned, an assumption about the deposit genesis will be made.

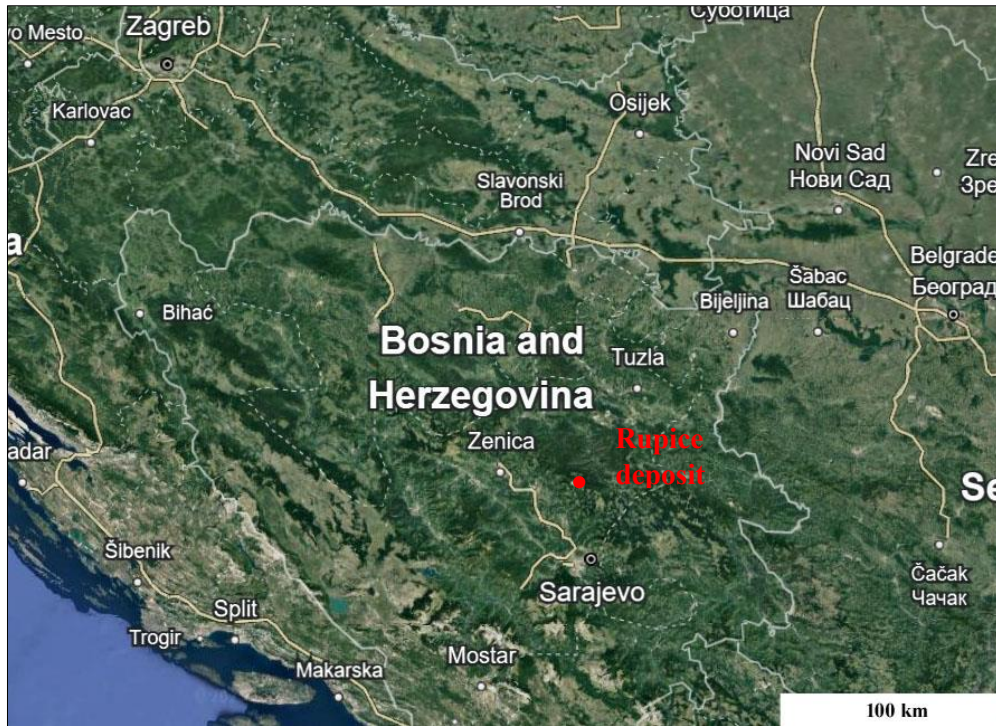


**Figure 1-1.** Location of the Rupice concession (obtained from Adriatic Metals Plc).

## 2. GEOGRAPHICAL SETTING

The Rupice deposit is located near the town of Vareš in the central part of Bosnia and Herzegovina (Fig. 2-1). Vareš is situated in the valley of the Stavnje River, within the Zvijezda mountain area (44.20°N, 18.30°E). It is part of the Zenica-Doboj Canton, one of the administrative regions of the Federation of Bosnia and Herzegovina. Larger towns near Vareš are Sarajevo, located about 45 km to the southwest of Vareš, and Zenica, situated to the west of Vareš, approximately 60 km away.

Vareš is situated within the Dinarides, so mountains and hills dominate the landscape. Stavnje River meanders through the area. Vareš boasts a relatively elevated position, primarily attributed to its mountainous surroundings. Elevation levels exhibit variability, typically between 800 and 1,000 meters above sea level across different sectors within the municipality.



**Figure 2-1.** Geographical position of study area (<https://earth.google.com/web/>).

### 3. GEOLOGICAL SETTING

#### 3.1. Regional geological setting

The Mediterranean region's geodynamic evolution is characterized by the ongoing interaction between the African and Eurasian tectonic plates, which began in the Mesozoic era. A better understanding of the geology in the Vareš mining region requires prior comprehension of the geological features of the central part of the surrounding Dinarides mountain range.

The metallogenic province of the Central Dinarides is part of the orogenic system of the Alpine-Himalayan chain, connected to the opening and subsequent closure of the Tethys Ocean that existed during the Mesozoic and the early Paleogene between two supercontinents - Eurasia or its Moesian fragment to the north and Africa or the Apulian (Adriatic) fragment to the south (Pamić et al., 1998). The geology of the Central Dinarides is described by the Alpine Wilson Cycle (Pamić et al., 1998);

- (1) Rifting processes spanned from Late Permian to Middle Triassic;
- (2) The opening of the oceanic Dinaridic Tethys began in the Late Triassic and lasted until the end of the Jurassic;

(3) Late Jurassic - Early Cretaceous initial subduction and thrusting of the Paleozoic – Triassic nappe onto ophiolites during the closure of the Dinaridic Tethys, accompanied by Alpine metamorphism;

(4) Late Eocene - Early Oligocene obduction of the ophiolite and the Paleozoic – Triassic nappe on the Adriatic – Dinaridic carbonate platform, with the development of the External Dinarides as a result.

From the SW to the NE, five tectonostratigraphic units are distinguished (Pamić et al., 1998) (Fig. 3-1);

- 1) The Adriatic - Dinaritic Carbonate Platform;
- 2) Passive continental margin carbonate–clastic tectonostratigraphic unit ('flysch bosniaque');
- 3) The Ophiolitic zone;
- 4) Formations related to the active continental margin (NW continuation of the Vardar zone);  
and
- 5) Paleozoic – Triassic nappes.

The Adriatic Carbonate Platform (ADCP) represents the External Dinarides, while the Internal Dinarides constitute Paleo – Mesozoic basement units, Dinaridic – ophiolitic zone, and formations of an active continental margin. The Palaeozoic – Triassic nappe occurs between the Internal and External Dinarides. Their frontal parts directly overlie the northeastern margin of the ADCP.

The Adriatic Carbonate Platform comprises the upper Paleozoic complex beneath layers of clastic sediments and platform carbonates from the Upper Permian to the Norian period, accompanied by volcanic rocks related to Triassic rifting activity. It also contains Norian–Lutetian carbonate platforms and Eocene oversteps flysch sequences.

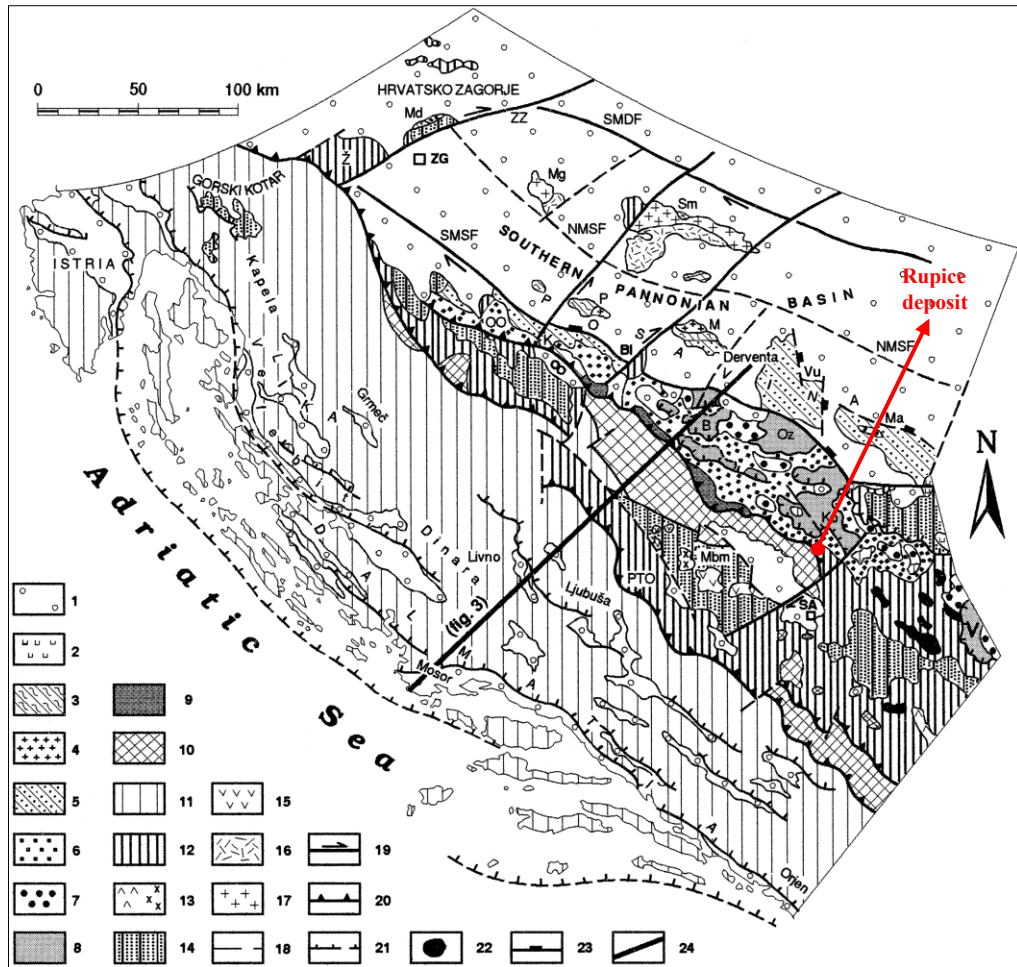
The Bosnian Flysch unit marks the development of a passive continental margin. Carbonate-clastic rocks were deposited on the continental slope and foothills of the Adriatic Dinaridic Carbonate Platform from the Jurassic to the Late Cretaceous. The Dinaride Ophiolite zone borders this geological formation to the northeast and the Paleozoic-Triassic nappe to the southwest.

The Ophiolite zone contains Mesozoic radiolarite with basalt effusions, an ophiolite complex with basalt and interlayers of greywacke and shale, ultramafic thrust sheets, and overstep sequences from the Late Jurassic to Late Cretaceous.

The sedimentary formations of an active continental margin were deposited within a trench and near a presumed magmatic arc. This geological formation experienced several subduction-related processes, which include sedimentation, magmatism, and metamorphism. It marks a suture zone positioned along the northern boundary of the Dinaridic branch of the Tethys Ocean. Within this zone, there are flysch sequences ranging from the Late Cretaceous to the Paleogene, incorporating volcanic units, tectonized ophiolite *mélange*, and regionally metamorphosed units derived from the surrounding Late Cretaceous to Paleogene rocks, along with synkinematic granitoids.

Palaeozoic – Triassic nappes, that are thrust onto the ophiolites, comprise metamorphic units from the Palaeozoic era, which have experienced varying degrees of metamorphism, and Triassic formations that conformably overlie Upper Permian sediments (Pamić et al., 1998).





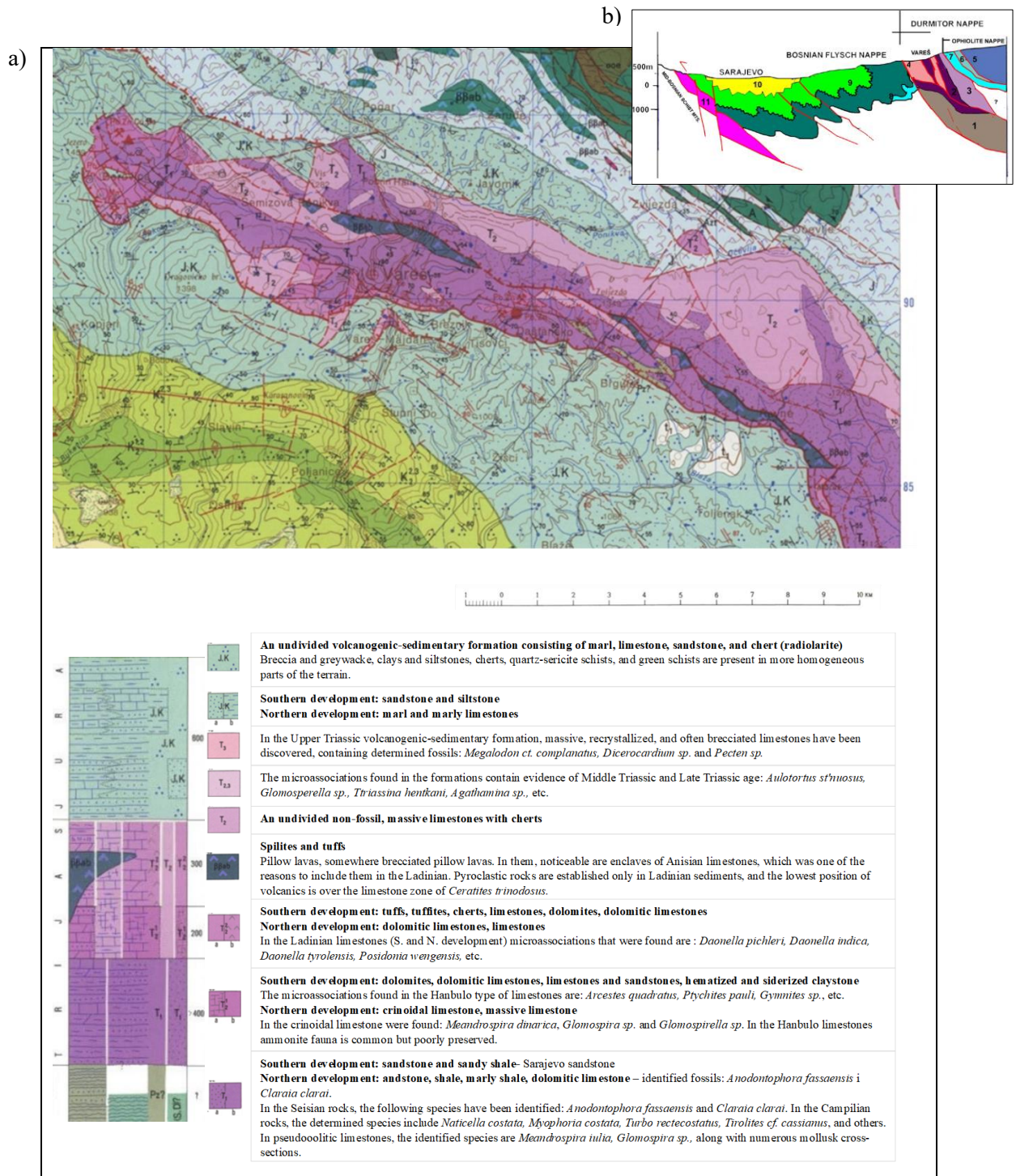
**Figure 3-1.** Geological map of the Central Dinarides. 1- Palaeogene–Neogene overstep sequences. 2- Tertiary volcanics. Active continental margin: 3- Mesoalpine metamorphic rocks; 4- Mesoalpine granitoids; 5- Upper Cretaceous–Palaeogene flysch; 6- Dinaridic Ophiolitic zone; 7- Late Jurassic–Late Cretaceous sequences unconformably overlying ophiolites; 8- large ultramafic massifs; 9- radiolarite sequence. Passive continental margin: 10- ‘flysch bosniaque’ and ‘zone prekarstique’; 11- ADCP. Palaeozoic–Triassic nappe: 12- allochthonous Triassic sequences; 13- Triassic volcanic and plutonic rocks; 14- allochthonous Palaeozoic sequences; 15- Palaeozoic volcanics. Tisia: 16- Hercynian progressively metamorphosed sequences; 17- Hercynian granitoids and migmatites (Pamić et al., 1998).

### 3.2. Local geological setting

At the beginning of the Alpine orogenesis, the Vareš area was submerged and represented the Tethyan sedimentary basin. Triassic and Jurassic sediments, deposited in the basin, have been thrust in a SW direction. The magmatism of advanced Triassic rifting produced spilites and ophiolitic basalts intercalated with Ladinian sedimentary rocks. The Rupice deposit is situated within the passive continental margin, as indicated by Pamić et al. (1998), or the northern part of the Durmidor nappe, as reported by Hrvatović (2000).

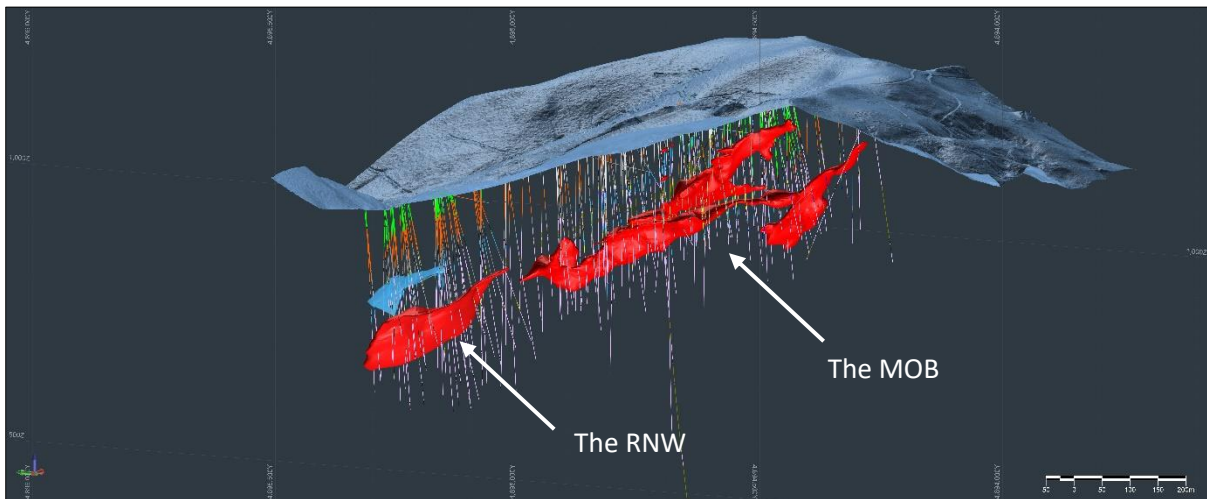
The Bosnian flysch nappe underlies the frontal parts of the Durmidor nappe, and the Ophiolite nappe overthrusts it. The Banja Luka-Sarajevo transversal fault's sigmoid shape defines the northern part of the Durmidor nappe. This geological zone is composed of Lower Triassic shales, sandstones, and limestones, Anisian limestones, and Ladinian spilites interbedded with pyroclastic rocks, cherts, shales, Fe-Mn shales, and, in some locations, covered with Upper Triassic carbonates (Hrvatović, 2000) (Fig. 3-2).

The sigmoid-shaped belt extending from Vareš-Borovica to Srednje-Draževici is host to various mineralizations formed in the time of Triassic rifting magmatism, such as cinnabar, Mn-oxide, monomineralic and polymetallic barite, as well as siderite-hematite mineralizations (Ramović et al., 1979).



**Figure 3-2. A)** Geological map and lithology of Vareš area (Pamić et al., 1978); **B)** Sarajevo-Vareš geological cross-section. Legend: 1-Eastern Bosnia Paleozoic; 2-Silica-clastic sediments of the Lower Triassic, 3-Anisian limestone, 4-Ladinian cherts, breccias, tuffs and limestone; 5-ophiolitic mélange; 6-"Wild" flysch; 7-Bosnian flysch Base; 8-J, K-paraflysch; 9-Upper Cretaceous and Paleogene flysch; 10-Sediments of the Sarajevo-Zenica Basin, 11-Triassic formations (Hrvatović, 2006).

The host rocks at Rupice consist of Middle Triassic limestone, dolostone, marl, and fine-grained siliciclastic rocks. The deposit has rich polymetallic mineralization (156 g/t Ag, 1.2 g/t Au, 4.3% Zn, 2.8% Pb, 0.4% Cu, 27% BaSO<sub>4</sub>) and a wide range of ore minerals, such as barite, galena, sphalerite, pyrite, chalcopyrite, and various sulfosalts. The identified Main Ore Body (MOB) extends 650m with an average true-width thickness of about 20m. Recent northwest drilling revealed a separate massive sulphide body called Rupice Northwest (RNW). RNW, situated at a lower stratigraphic level than MOB, is interpreted as overlapping but not connecting with MOB (Fig. 3-3). RNW has a current strike extent of approximately 250m, with mineralization remaining open in most directions. The footwall zone of RNW is pervasively silica-sericite altered, containing finely disseminated sulphides, base metal stringer zones, and mineralized faults/shears. This alteration zone appears enriched in zinc. Approximately 90m to 100m above Rupice NW, on the hanging wall, there is a horizon with high base metal content referred to as the Upper Zone, which has low barite and is rich in pyrite. It occurs as a matrix in a dolomite/limestone breccia (Adriatic Metals Plc, 2022).



**Figure 3-3.** Ore body model of the Rupice deposit (until April 2023) (Adriatic Metals Plc).

#### 4. SAMPLING AND ANALYTICAL METHODS

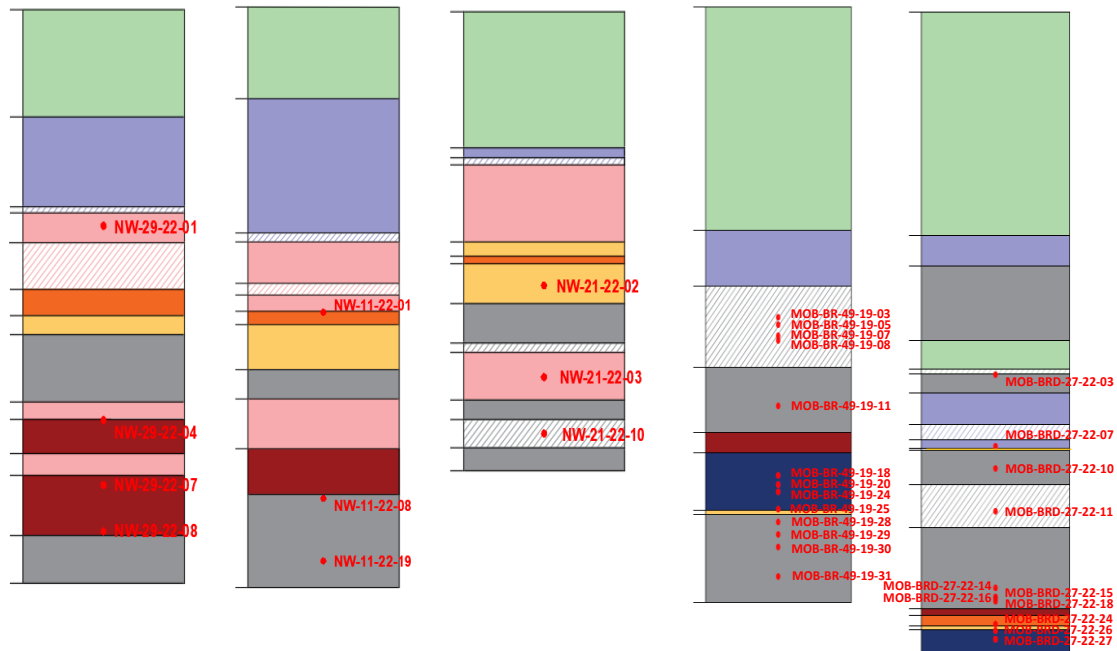
Five representative drill cores were selected based on the following criteria: (a) geographical position of the drill core within the exploitation field, (b) appearance of mineralization in the main ore body (MOB) and Rupice Northwest (NW), and (c) associated rocks and macroscopic fabrics. A total of ninety-nine samples were sampled from selected cores: NW-29-22-(samples 01 to 07), NW-21-22-(samples 01 to 10), NW-11-22-(samples 01 to 19), MOB-BR-49-19-(samples 01 to 31), MOB-BRD-27-22-(samples 01 to 30), and MOB-BR-04-20-02.

Thirty-six thin sections from host rocks were examined under an optical microscope. X-ray diffraction was made on eleven samples, which were also analysed using the X-ray fluorescence method (Table 4-1).

**Table 4-1.** List of chosen representative samples and conducted analyzes.

Sample	Sample description	From [m]	To [m]	Optical petrology	Colouring	XRD	XRF
MOB-BRD-27-22-10	Siliciclastic – carbonate facies	267	267,1	+		+	+
MOB-BRD-27-22-11		292	292,1	+			
MOB-BRD-27-22-14-A		319,5	319,6	+	+	+	+
MOB-BRD-27-22-14-B		319,5	319,6	+	+	+	+
MOB-BRD-27-22-15		342	342,2	+		+	+
MOB-BRD-27-22-16		343,4	343,6	+	+	+	+
MOB-BRD-27-22-18-A		344,6	344,8	+			
MOB-BRD-27-22-18-B		344,6	344,8	+			
MOB-BRD-27-22-26		361,70	361,80	+	+		
MOB-BR-49-19-03		178,40	178,55	+	+		
MOB-BR-49-19-05		182,60	182,80	+	+		
MOB-BR-49-19-07		189	189,2	+	+		
MOB-BR-49-19-08		191,7	191,9	+	+		
MOB-BR-49-19-11		229,40	229,60	+			
MOB-BR-49-19-20		274,7	274,85	+		+	+
MOB-BR-49-19-28		296,20	296,40	+	+		
MOB-BR-49-19-29		303,40	303,60	+	+		
MOB-BR-49-19-30		310,60	310,75	+	+		
MOB-BR-49-19-31		327,60	327,80	+			
NW-29-22-04		238	238,1	+		+	+
NW-11-22-01	206,50	206,60	+				
NW-11-22-08	332,6	332,7	+		+	+	
NW-11-22-19	374,80	375,00	+				
NW-21-22-10	244,3	244,4	+				
NW-21-22-02	Dolomitic breccia	158,5	158,6	+			
BR-04-20-02	Spilite facies	254,50	254,80	+			
MOB-BRD-27-22-27		366,8	366,9	+			
MOB-BR-49-19-18		269,4	269,6	+			
MOB-BR-49-19-24		278,80	278,95	+		+	+
MOB-BR-49-19-25		288,90	289,10	+		+	+
MOB-BRD-27-22-24	Mineralized breccia (Upper mineralization zone)	358	358,2	+		+	+
NW-29-22-07		273,40	273,50	+			

NW-29-22-08	Main mineralization zone	300,00	300,20	+			
NW-21-22-03	Chert facies	211,6	211,7	+			
NW-29-22-01		124,20	124,30	+			
MOB-BRD-27-22-03	Limestone facies	217,1	217,2	+	+		



**Figure 4-1.** Red spots indicate the position of the petrographic thin section within drill-cores.

#### 4.1. Polarized light microscopy

Polarized light is a non-destructive method used to identify the mineral composition of the samples, the difference between features of certain mineral phases within, classify rocks, paragenetic sequences, and alteration processes, and get an insight into rock-forming conditions. The thin sections for optical microscopy were prepared using a standard procedure. The samples were cut into 30 µm plates and polished, after which they were cemented with Canada balsam to glass slides. Microscopic photographs were taken using the OPTICA B-1000 POL polarization microscope at the Faculty of Mining, Geology and Petroleum Engineering, University of Zagreb.

#### 4.2. Colouring of the carbonates

The method of carbonate staining is a commonly used, fast, and simple technique for identifying carbonates. It is based on the reaction between a specific solution and a rock or

mineral, resulting in colouration that indicates the composition (Table 4-2). There are various types of carbonate staining methods. The Alizarin Red S solution and potassium ferrocyanide solution methods were used. The specimen is immersed in 1.5% HCl, in distilled water, stained, and then dipped in a mixture of Alizarin Red S and potassium ferrocyanide solutions in a 3:2 ratio (Dickson, 1965).

**Table 4-2.** Stainings and minerals are indicated by the carbonate staining procedure.

<b>Mineral</b>	<b>Staining</b>
Calcite	Red colouring
Fe-calcite	Purple colouring
Dolomite	Colourless
Fe-dolomite	Turquoise colouring

### **4.3. X-ray diffraction analysis**

To determine the mineralogical composition of samples, an X-ray diffraction (XRD) analysis was conducted. When an X-ray beam interacts with a sample and undergoes diffraction, applying Bragg's Law allows us to determine the distances between the atomic planes within the sample, which is expressed as  $n\lambda = 2d\sin\theta$ .

Here, 'n' represents the order of the diffracted beam, ' $\lambda$ ' is the wavelength of the incident X-ray beam, 'd' stands for the distance between adjacent atoms, and ' $\theta$ ' is the angle at which the X-ray beam is incident. The characteristic set of d-spacings obtained during a typical X-ray scan provides a distinct "fingerprint" of the mineral phase or phases present in the sample.

These selected samples were ground using an agate set to create a powdered fraction. XRD analysis was performed using a Malvern PanAnalytical vertical X-ray goniometer (X'Pert MPD model) equipped with a Cu tube and a graphite crystal monochromator. The experimental conditions included 45 kV, 40 mA, automatic primary beam divergence, an irradiated length of 0.5 mm, and a continuous scan with a step size of  $0.0131303^\circ$  2 $\theta$ /s. The data obtained from the analysis was then analyzed using the X'Pert HighScore plus 2.1 PANalytical B.V. software.

### **4.4. X-ray fluorescence analysis**

An X-ray fluorescence (XRF) analysis was carried out using a portable energy-dispersive XRF analyzer. It is a non-destructive analytical technique used to determine the elemental composition of minerals. Each of the elements present in a sample produces a set of characteristic fluorescent X-rays that is unique for that specific element. The table of results

shows the pseudo-total concentrations in percentages (%) and parts per million (ppm) for 20 elements, including Si, Ti, Cr, Al, Fe, Mn, Mg, Ca, K, Rb, Sr, Ba, Cu, Ag, Zn, Pb, Cd, P, As, and S.

#### **4.5. Fossils age determination**

Examining fossil-containing samples involved the analysis of thin sections using a Leica DM-LSP polarization microscope. The extraction of well-preserved radiolarian fossils from a sample was carried out using a 5% diluted hydrofluoric acid method (Pessagno and Newport 1972; De Wever et al. 2001). These fossils were studied using a Scanning Electron Microscope, and their dating was determined following the Catalogue of Mesozoic radiolarian genera (O'Dogherty et al. 2009), as well as the revision of the Nassellarian family Tetrastropocystidae (Dumitrica, 2017). The foraminifera assemblages were analysed by plane polarizing light microscopy using a Leica DM-LSP polarization microscope (Conducted by Dujе Kukoč, PhD and Tonči Grgasović, PhD).



## 5. RESULTS

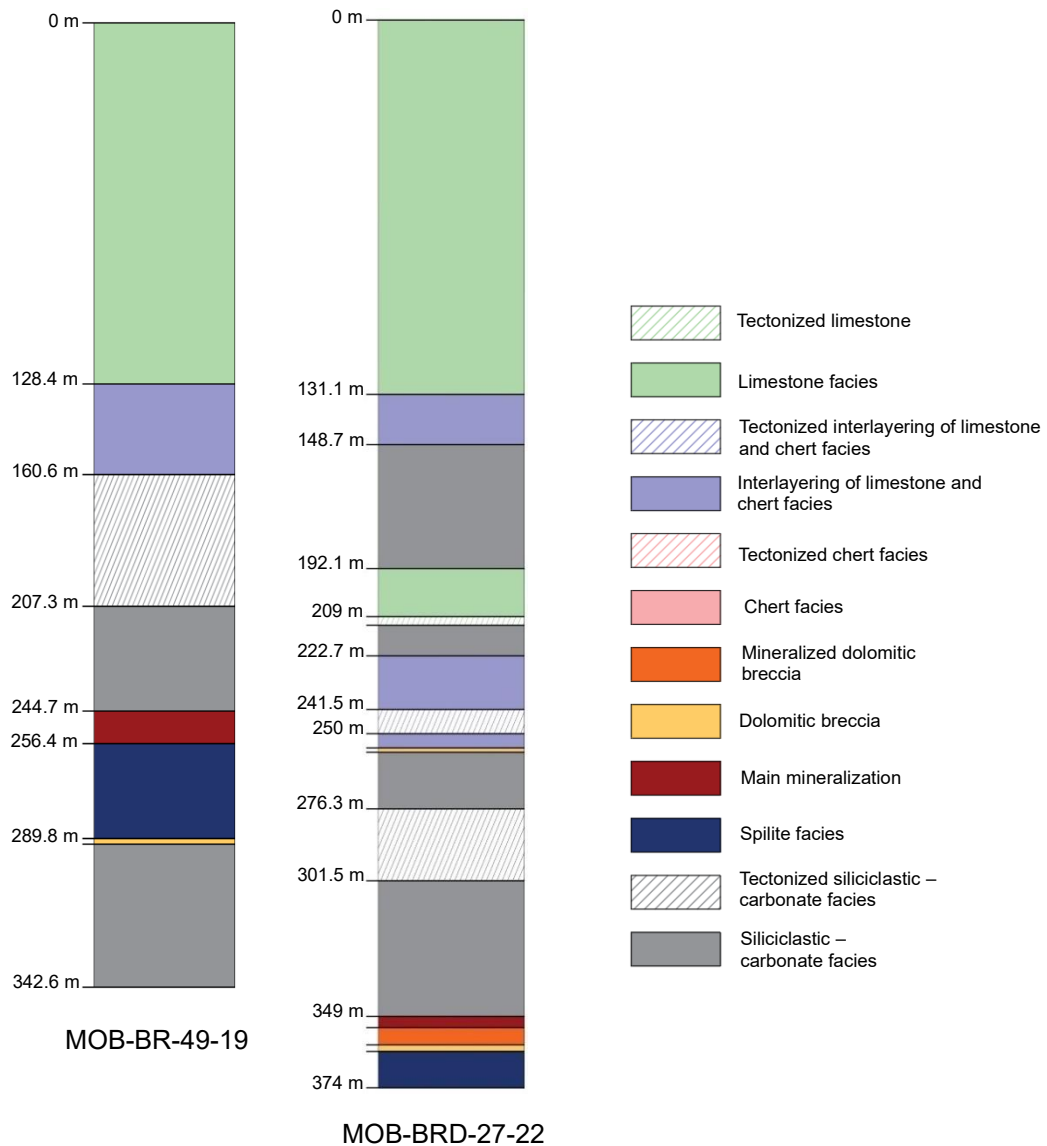
The results of the research will be presented in separate sections. The first part of the results will showcase the field determination of facies found in the drill holes, along with their corresponding descriptions. It will be followed by the results of the micro petrographic analysis for each facies and its associated lithotypes. The X-ray diffraction results will be used to supplement the information obtained from micropetrographic data. The geochemical results will detail the XRF analyses conducted on the whole rock. Finally, the age determination based on index fossils will be shown.

### 5.1. Field study

Different structure characteristics are observed between the MOB and RNW ore bodies. The MOB exhibits the Main mineralization zone, whereas RNW displays the Main and the Upper mineralization zones. The cores were mapped from the deeper section towards the shallower. Seven facies were differentiated: a) siliciclastic – carbonate facies, b) chert facies, c) spilite facies, d) Main mineralization zone, e) dolomite breccia facies, f) mineralized dolomitic breccia (Upper mineralization zone), and g) limestone facies. They appear in one to tens of meters thick intervals in the drill cores.

#### *The Main Ore Body Rupice*

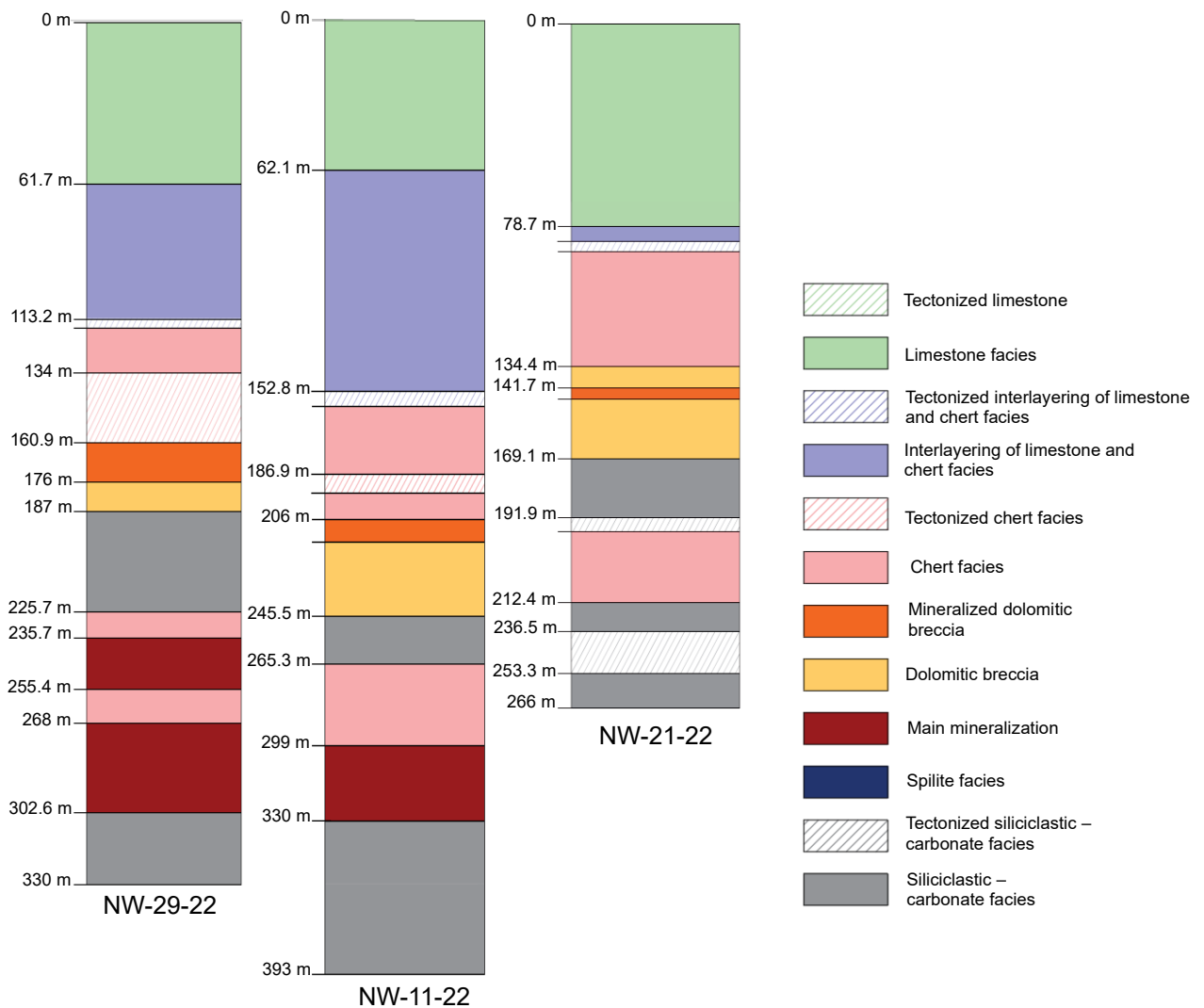
The ore-bearing layer displays the zonation of massive ore minerals. The mineralization zone and footwall contact are stratigraphic, while contact with the hanging wall is tectonized. The footwall's deepest drilled lithological unit is siliciclastic-carbonate facies. Above this unit, spilite and basalt are deposited, with tuff and chert overlaying it. In the drill core MOB-BR-49-19, a massive dolomitic unit intersects spilite. The hanging wall marks a tectonized siliciclastic-carbonate unit, similar to those in the footwall of the deposit, covered by a package of limestones and cherts (Fig. 5-1).



**Figure 5-1.** Lithological units of the MOB.

*The Rupice Northwest ore body*

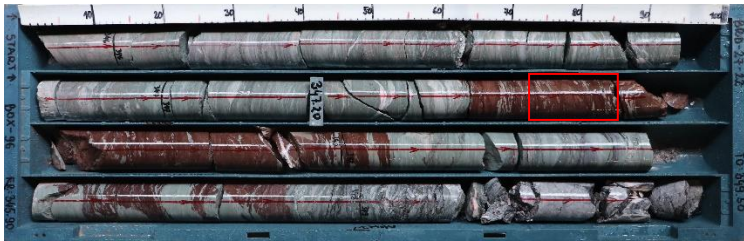
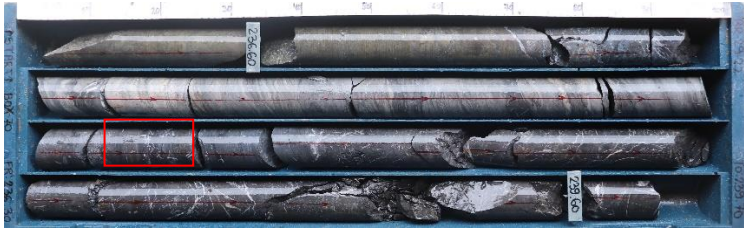
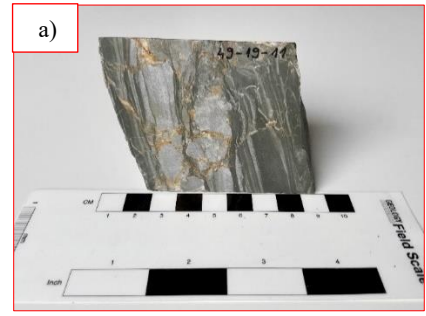
The Main mineralization body exhibits ore zonation and displays sharp contact with surrounding rocks. The Upper mineralization zone is hosted by dolomitic breccia and is in tectonic contact with host rocks. In the footwall, the deepest unit consists of a highly tectonized siliciclastic-carbonate unit. It is covered by chert host rock, crosscut by stockwerks in the drill cores NW-11-22 and NW-21-22. Between two mineralization zones lies a sequence of a chert lithotype overlaid by a siliciclastic-carbonate unit. Both units have similar characteristics to the ones in the footwall. A sequence of chert, limestone, and marl marks the hanging wall of the deposit (Fig. 5-2).

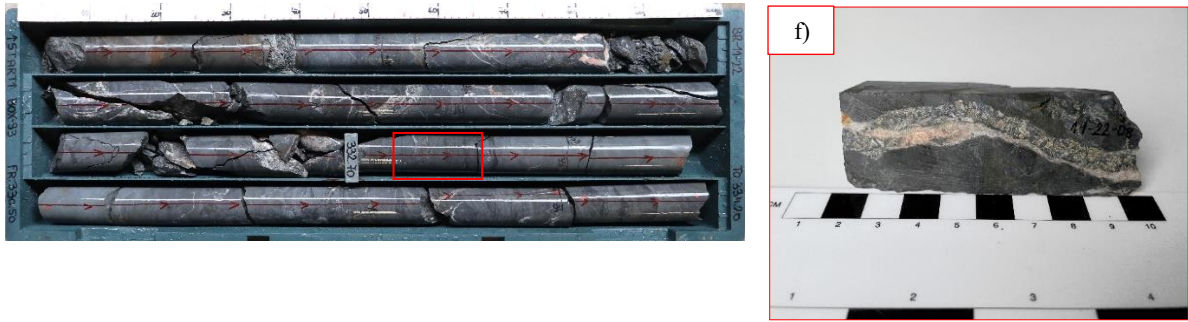


**Figure 5-2.** Lithological units of the NW ore body.

### 5.1.1. Siliciclastic – carbonate facies

Siliciclastic – carbonate facies appears in the footwall and hanging wall of the deposit. It has a laminated texture, intersected with calcite veins. Pale layers contain a higher percentage of carbonate components than darker ones (Fig. 5-3. A, B). It can exhibit a red colour due to hematitization (Fig. 5-3. C). In contact with mineralization, fine-grained pyrite and carbonate fragments replaced by pyrite can be recognized (Fig. 5-3. E). In the footwall, the unit is crossed by a stockwork filled with medium-crystalline barite, galena, sphalerite, pyrite, and rhodochrosite (NW-21-22 and NW-11-22) (Fig. 5-3. F). Massive dolostone is present in the footwall of the MOB-BR-49-19 (Fig. 5-3. D). It has a purplish colour due to hematitization, and is crosscut with calcite veins.

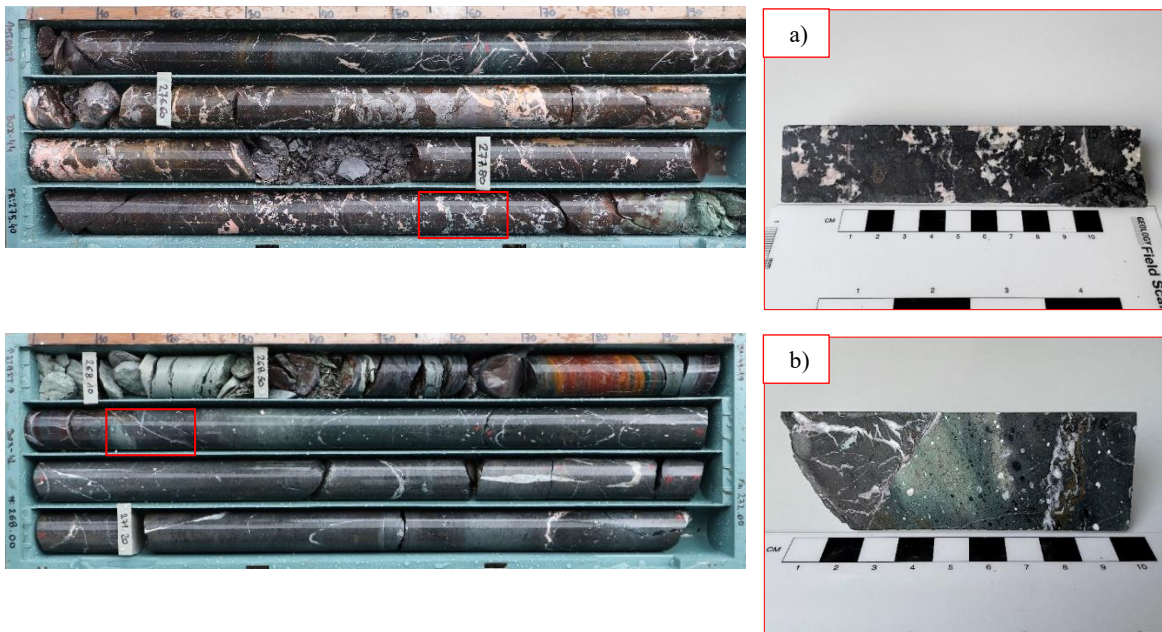




**Figure 5-3.** The position of the samples **A)** MOB-BR-49-19-11, **B)** NW-29-22-04, **C)** MOB-BRD-27-22-15, **D)** MOB-BR-49-19-20, **E)** NW-11-22-01, and **F)** NW-11-22-08 is framed by the red rectangle (left figure obtained from Adriatic Metals Ptc.).

### 5.1.2. Spilite facies

Spilite facies is present in the footwall unit of the MOB. Macroscopically, three types of spilite formations are recognized –brecciated spilite with irregular amygdalas, basalt with rounded voids, and pyroclastic rock. Fragmented spilite is cemented with calcite, rhodochrosite and celadonite. Spilite consists of plagioclase phenocrysts within the matrix (Fig. 5-4. A). Colour varies from red due to hematitization, to green due to celadonite and chlorite presence. Basalt has a vesicular texture and light to dark green-purple colour (Fig. 5-4. B). It has regular, rounded voids filled with calcite, chlorite and celadonite. Two types of tuffs can be recognized. Dark green, compact tuffs with visible layering (sample MOB-BRD-27-22-27) (Fig. 5-4. C), and friable, pale green varieties with a shale texture.

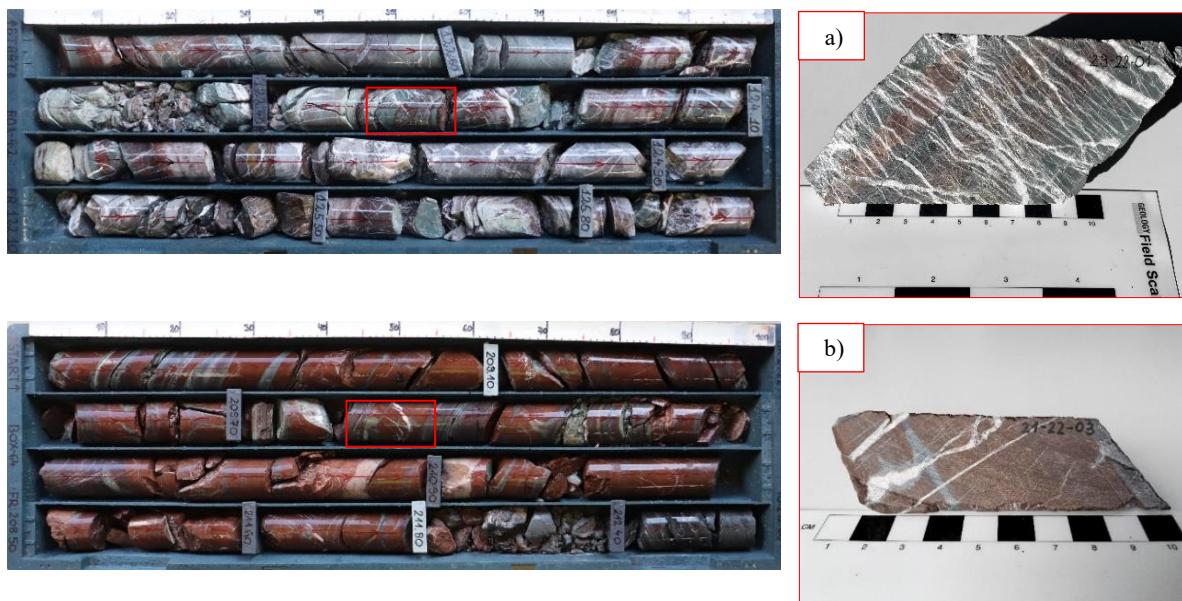




**Figure 5-4.** The position of the sample **A)** MOB-BR-49-19-25, **B)** MOB-BR-49-19-18, **C)** MOB-BRD-27-22-27 is framed by the red rectangle (left figure obtained from Adriatic Metals Ptc.).

### 5.1.3. Chert facies

The chert facies is characterized by a homogeneous texture. It overlies massive mineralization in the drill holes NW-29-22 and NW-11-22, and intersects the siliciclastic-carbonate unit in the drill hole NW-21-22. Unaltered chert has a dark grey colour (Fig. 5-5. A), while altered chert exhibits a red colour due to hematitization (Fig. 5-5. B). Tensional white calcite veinlets crosscut this unit.



**Figure 5-5.** The position of the samples **A)** NW-29-22-01 and **B)** NW-21-22-03 is framed by the red rectangle (left figure obtained from Adriatic Metals Ptc.).

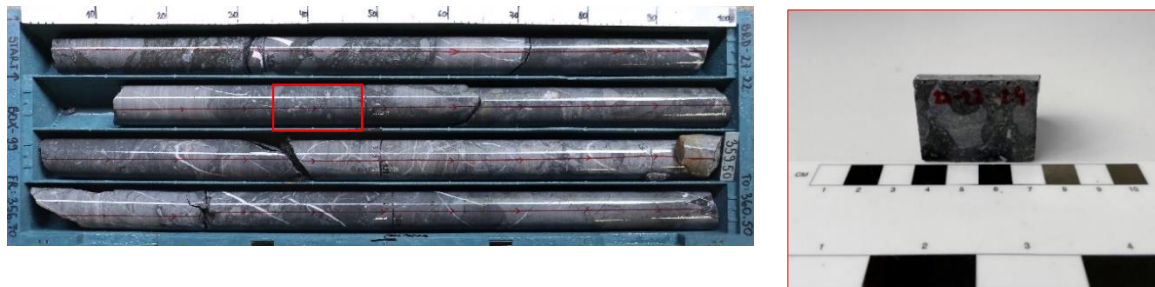
### 5.1.4. Ore – bearing facies (the Main and the Upper mineralization zone)

The Main mineralization body exhibits zonation from massive sulphide to massive barite (absent in the drill core NW-21-22). Drill core MOB-BRD-27-22 exhibits zonation from dolomitic breccia with a mineralized matrix, followed by massive sulphide to massive barite

mineralization. A wide range of ore minerals are identified - barite, galena, sphalerite, pyrite, and cinnabar.

The Upper mineralization zone is hosted by dolomitic breccia (Fig. 5-6. A). Various fabrics of mineralization occur:

1. A mineralized matrix containing an idiomorphic barite crystal, small clusters of sphalerite and galena, or sphalerite, galena, and pyrite impregnation, and
2. A carbonate fragments replaced by disseminated pyrite.



**Figure 5-6.** The position of the sample MOB-BRD-27-22-24 is framed by the red rectangle (left figure obtained from Adriatic Metals Ptc.).

#### 5.1.5. Dolomitic breccia facies

The dolomitic breccia unit consists of dark grey angular to sub-angular dolomitic fragments within a black matrix and varies from clast-supported to matrix-supported breccia (Fig. 5-7). Fine-grained pyrite can be identified in the black cement beneath the mineralized dolomite breccia.



**Figure 5-7.** The position of the sample NW-21-22-02 is framed by the red rectangle (left figure obtained from Adriatic Metals Ptc.).

#### 5.1.6. Limestone facies

In the MOB and the RNW limestone is present in the hanging wall. The texture ranges from massive to laminated, with interlayers of chert and brecciated carbonate fragments (Fig.

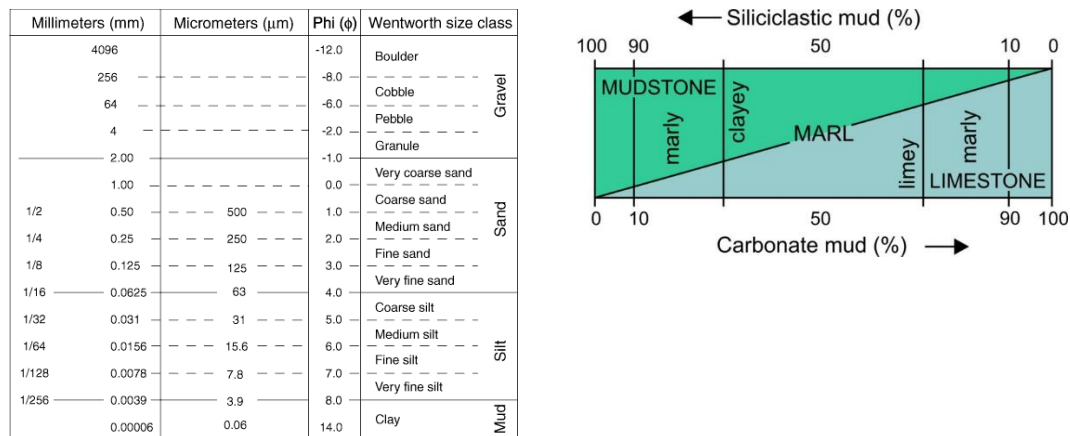
5-8). Its visual appearance is diverse, displaying shades of greyish, pinkish, yellowish, and brownish, which can be attributed to weathering. Visible mineralization tracks within the limestone facies is not apparent.



**Figure 5-8.** The position of the sample MOB-BRD-27-22-03 is framed by the red rectangle (left figure obtained from Adriatic Metals Ptc.).

## 5.2. Polarized light microscopy

Based on microscopic investigation of 36 thin sections 14 lithotypes (LT) were differentiated: dolomitic marl (LT1A), silicified marl (LT2B), dolomitic siltstone (LT2A), silicified siltstone (LT2B), dolomitic (LT3A), LD dolomite (LT3B), tuff (LT4), amygdaloidal basalt (LT5), spilite breccia (LT6), radiolarite (LT7), barite-sulphide mineralization (LT8), mineralized dolomitic breccia (LT9), dolomitic breccia (LT10), and mudstone (LT11). The classification is made up according to Fig. 5-9. In the lithotype names sand, silt and clay refer to grain sizes, and shale stands for structure type. They are described in detail in the following sections.



**Figure 5-9.** a) Classification and nomenclature of clastic sediments based on grain size (Wentworth, 1922); b) Classification of marls based on the proportion of siliciclastic and carbonate mud (Compton, 1962).



### 5.2.1. Siliciclastic-carbonate facies

In the siliciclastic-carbonate facies, three lithotypes are defined based on grain size and the proportion of siliciclastic and carbonate components – Marl, siltstone, and dolomite.

#### 5.2.1.1. Lithotype 1 (LT1): Marl

In this lithotype, two subtypes were determined based on the absence and presence of secondary silicification, sericitization and framboidal pyrite.

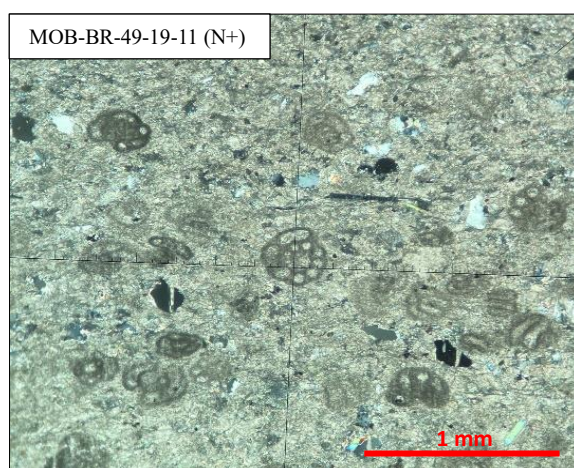
##### *Lithotype 1A (LTA1): Dolomitic marl*

The typical mineralogical phases of the laminated dolomitic marl are dolomite and quartz, while white mica forms a minor fraction (Table 5-1). Zircon occurs in some samples and fossils, such as foraminifers and thin-shelled molluscs (Fig. 5-10). Thin sections exhibit rhythmic alteration between dolomite-quartz and sericite laminae. Sample MOB-BR-49-19-11 consists of sandstone interlayers approximately 0.12 mm thick.

Irregular **quartz** grains are fresh with undulose extinction. The interference colour is white of I. order. Contact with other mineral phases exhibits from sharp to irregular. The size of grains varies from 0,004x0,004 to 0,008x0,012 mm. **Dolomite** is a primary carbonate mineral present in the marl rock. It has an idiomorphic to allotriomorphic, rhombohedral habit of clayey dimensions. Dolomitic crystals show distinct relief changes and have poor to no visible cleavage. The interference colour is white of the higher order. **White mica** has a hypidiomorphic tabular habitus. Interference colour is brilliant of II-III. order with an extinction angle of 0 – 3°.

**Table 5-1.** Mineral composition of dolomitic marl.

Sample	Structure	Mineral composition					
		Dolomite	Quartz	Calcite	White mica	Zircon	Fossils
BRD 49-19-11	Laminated	55%	20%	15%	10%	/	foraminifers
BRD 49-19-31	Laminated	50%	20%	20%	10%	/	/
NW-11-22-19	Laminated	60%	30%	/	10%	1%	thin-shelled molluscs



**Figure 5-10.** Thin section micro-photographs of dolomitic marl sample MOB-BR-49-19-11 containing foraminifera within fine dolomite, quartz, calcite, and white mica.

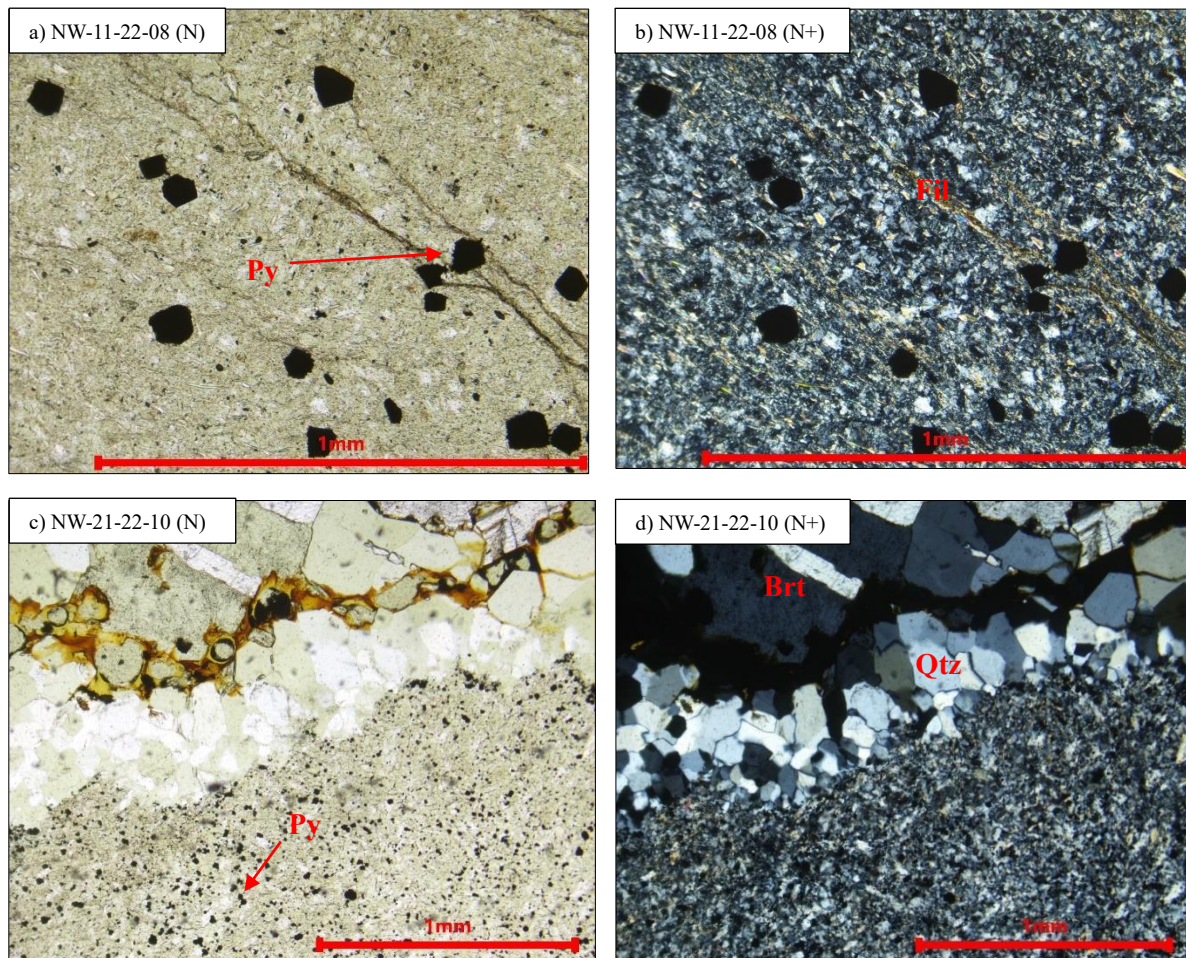
*Lithotype 1B (LTB): Silicified marl*

Thin sections of silicified marl are primarily composed of closely packed quartz crystals (Table 5-2). The minor fraction is sericite and framboidal pyrite, with barite in sample NW-11-22-08 (Fig. 5-11). Accessory zircon is present in the sample NW-11-22-08.

Allotriomorphic **quartz** crystal boundaries are cloudy and undefined. Quartz has undulose extinction, and the interference colour is white of I. order. Dimensions exhibit from 0,004x0,004 to 0,008x0,012 mm. **Sericite** is present between quartz crystals. It has a hypidiomorphic tabular habitus, from 0,004x0,004 mm to 0,008x0,012 mm in size. Interference colour is brilliant of II-III. order with an extinction angle of 0 – 3°. **Framboidal pyrite** has idiomorphic to hypidiomorphic, pyritohedral grain form with dimensions from 0,01x0,01 to 0,06x0,06 mm. **Barite** is present in the mineralized vein as hypidiomorphic to allotriomorphic tabular crystals. It is colourless with moderate positive relief. With XPL, it shows grey and white to yellow interference colour of I. order and parallel extinction. Crystal size ranges between 0,005x0,01 mm to 0,07x0,3 mm.

**Table 5-2.** Mineral composition of silicified marl.

Sample	Structure	Mineral composition					
		Quartz	Sericite	Pyrite	Barite	Opaque mineral	Zircon
NW-11-22-08	Massive	60%	5%	7%	20%	≈10%	<1%
NW-21-22-10	Laminated	80%	15%	7%	/	/	/



**Figure 5-11.** Thin section micro-photographs of silicified marl: **A, B)** fine-crystalline quartz, sericite, and framboidal pyrite; **C, D)** coarse quartz crystals at the contact of idiomorphic, tabular barite and very fine quartz, sericite and framboidal pyrite dispersed within matrix.

#### 5.2.1.2. *Lithotype 2 (LT2): Siltstone*

In this lithotype two subtypes were determined based on the absence and presence of secondary silicification, sericitization, and framboidal pyrite appearance.

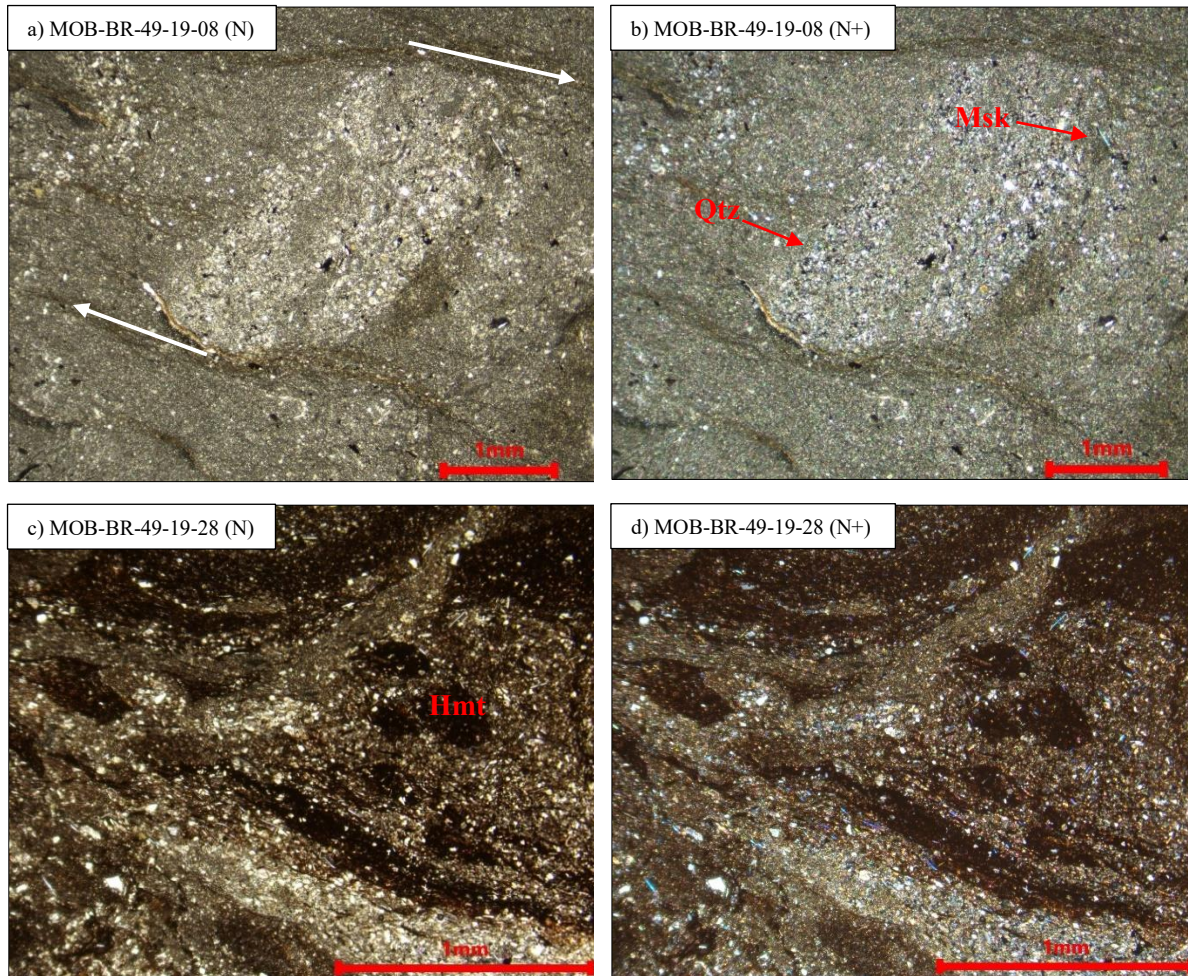
##### *Lithotype 2A (LT2A): Dolomitic siltstone*

The main composition of the siltstone are dolomitic particles with dimensions less than 0,063 mm. Quartz and white mica are forming minor fraction. In the siltstone occasionally are found limestone fragments and sandstone pockets in which quartz, dolomite, calcite, and white mica are cemented with very fine dolomite (Table 5-3). Hematite is present as a secondary mineral (Fig. 5-12. C, D). The rocks commonly exhibit a shale structure, although the laminae are often disturbed. In the MOB-49-19-08 they are indicating the shear direction (Fig. 5-12. A, B). Occasionally, accessory zircon can be found.

Allotriomorphic **quartz** has undulatory extinction and grey interference colour of I. order, approximately 0,004x0,005 mm in size. Hypidiomorphic to idiomorphic rhombohedral **dolomite** crystals are around 0,0015x0,0025 mm in size. **Calcite** is primarily present as crystalline vein and pore filling. It is recognized by red coloration. **White mica** has tabular hypidiomorphic habitus, 0,005x0,01 mm in size. Interference colour is brilliant of II-III. order with an extinction angle of 0 – 3°.

**Table 5-3.** Mineral composition of dolomitic siltstone.

Sample	Structure	Mineral composition						
		Dolomite	Quartz	Calcite	White mica	Hematite	Opaque minerals	Zircon
MOB-BR-49-19-07	Shale	50%	15%	15%	15%	/	5%	/
MOB-BR-49-19-08	Shale	50%	25%	10%	10%	5%	/	/
MOB-BR-49-19-28	Shale	40%	15%	5%	10%	25%	5%	/
MOB-BR-49-19-29	Shale	50%	25%	10%	10%	/	5%	/
MOB-BRD-27-22-10	Shale	45%	25%	10%	20%	/	/	/
MOB-BRD 27-22-15	Shale	50%	20%	10%	5%	15%	/	1%
MOB-BRD 27-22-18a	Shale	60%	15%	15%	10%	/	/	/
MOB-BRD 27-22-18b	Shale	55%	20%	15%	10%	/	/	/



**Figure 5-12.** Thin section micro-photographs of dolomitic siltstone: **A, B**) white arrows pointing shear directions and foliation texture in dolomitic siltstone; **C, D**) hematitized dolomitic siltstone.

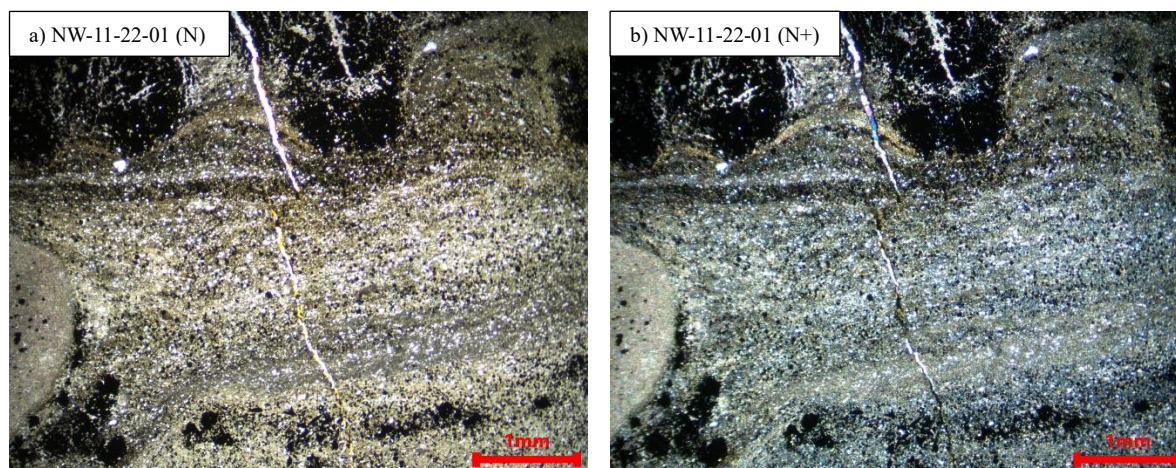
*Lithotype 2B (LT2B): Silicified siltstone*

In thin sections some laminae are rich in quartz and framboidal pyrite, whereas others consist mostly of dolomite and white mica (Table 5-4). Imprinted, occasionally pyritized, limestone fragments can be observed in the siltstone, evidenced by laminae folding at the contact of the fragment and the rock (Fig. 5-13).

**Quartz** exhibits allotriomorphic habitus. It has undulatory extinction and I. order grey interference colour. Grain dimensions are approximately 0,0025x0,003 mm. **Dolomite** has hypidiomorphic to idiomorphic rhombohedral habitus, 0,002x0,003 mm in size. **Calcite** is primarily present as vein-filling, but as a minor component of marl paragenesis. The thickness of the veins is approximately 0,1 mm. **White mica** has a tabular hypidiomorphic habitus. Interference colour is brilliant of II-III. order with an extinction angle of 0 – 3°. Grain dimensions range from 0,002x0,004 to 0,002x0,02 mm. **Pyrite** is opaque in thin sections and has idiomorphic to hypidiomorphic, pyritohedral grain form.

**Table 5-4.** Mineral composition of silicified siltstone.

Sample	Structure	Mineral composition							
		White mica	Pyrite	Quartz	Dolomite	Calcite	Zircon	Rutile	Plagioclase
NW-11-22-01	Shale	20%	47%	25%	5%	/	1%	1%	1%
MOB-BRD 27-22-14a	Shale	35%	20%	25%	10%	10%	/	/	/
MOB-BRD 27-22-14b	Shale	35%	15%	30%	20%	/	/	/	/



**Figure 5-13.** Thin section micro-photographs of sample NW-11-22-01; quartz-pyrite and sericite laminae folding in the silicified siltstone.

5.2.1.3. *Lithotype 3 (LT3): Dolomite*

In this lithotype, two subtypes were differentiated based on the grain size of the dolomite: dolomicrite, and late-diagenetic dolomite. Both dolomites are cut across by red-stained calcite and quartz veins.

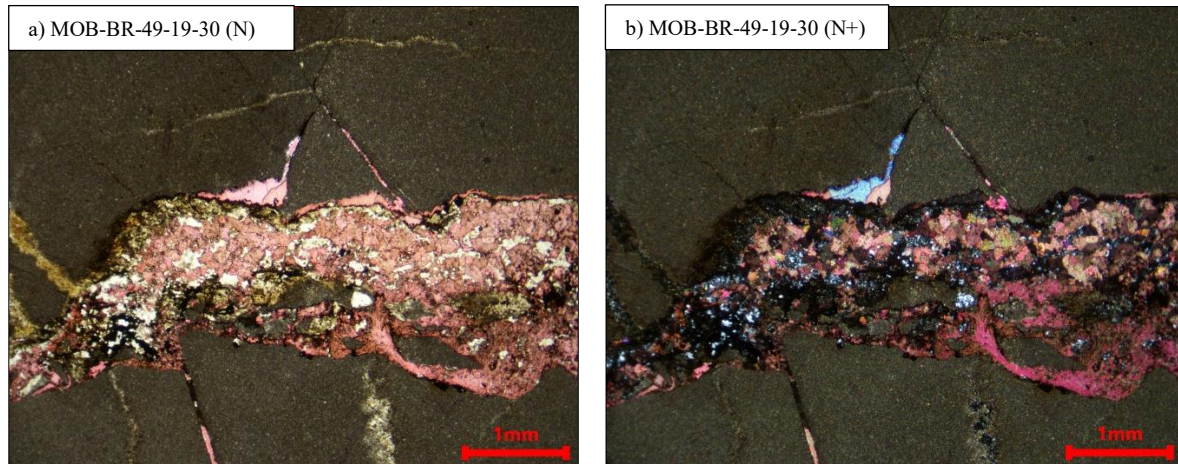
*Lithotype 3A (LT3A): Silty, clayey dolomicrite lithotype*

The dolomicrite contains irregular non-ferroan dolomite, silty to clayey in size. White mica and Fe-oxides form a minor phase (Table 5-5). Quartz and calcite are present as a crystalline filling in the veins that crosscut dolomicrite. Boundaries among dolomite crystals are mainly undeterminable (Fig. 5-14).

**Table 5-5.** Mineral composition of silty, clayey dolomicrite.

Sample	Structure	Mineral composition				
		Dolomite	Fe-oxides	Quartz	Calcite	White mica
MOB-BR-49-19-03	Breccia	65%	15%	/	20%	/
MOB-BR-49-19-05	Breccia	70%	15%	/	15%	/

MOB-BR-49-19-30	Homogenous	70%	5%	25%	/	/
MOB-BRD-27-22-11	Homogenous	65%	5%	25%	/	5%



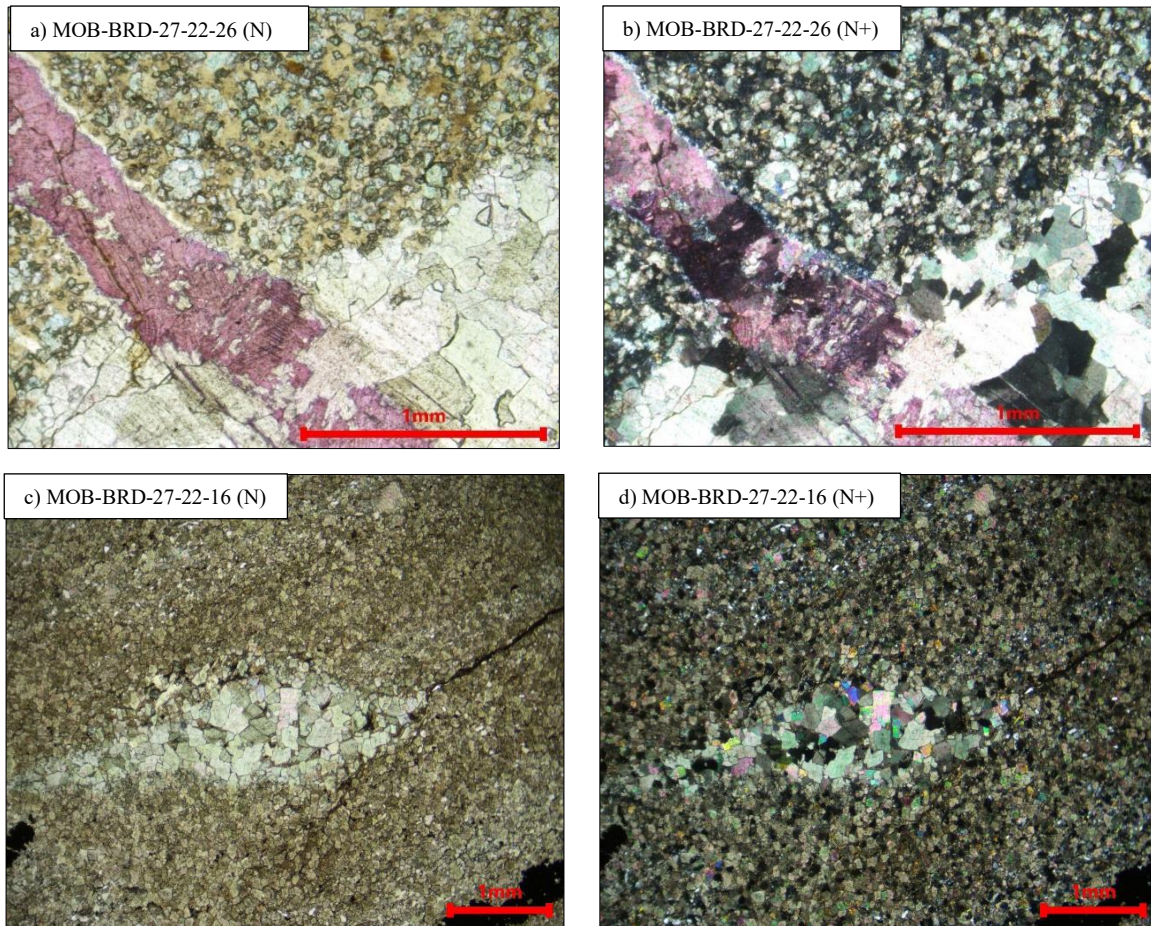
**Figure 5-14.** Thin section micro-photographs of silty, clayey dolomitic intersected by partially oxidized, red stained calcite and quartz vein.

*Lithotype 3B (LT3B): Silty, sandy LD dolomite lithotype*

The LD dolomite comprises closely packed idiomorphic to hypidiomorphic dolomite crystals with sizes of approximately 0.015x0.0175 mm (Table 5-6). The intercrystalline pores contain Fe-oxide aggregate and clayey minerals, indicating a cement-supported fabric (MOB-BR-49-19-20, MOB-BRD-27-22-16) (Fig. 5-15. C, D). In the MOB-BRD-27-22-26, coarse dolomite crystals are “floating” in the very fine quartz indicating silicification (Fig. 5-15. A, B). Two dolomite textures are recognized; **Dol1** stands for non-ferroan coarse dolomite, and **Dol2** for blue-coloured, microcracks- and partially matrix-filling, ferroan dolomite-ankerite. Sample MOB-BR-49-19-20 was not coloured for the purpose of carbonate identification.

**Table 5-6.** Mineral composition of silty, sandy LD dolomite.

Sample	Structure	Mineral composition			
		Dolomite	Quartz	Fe-oxides	Calcite
MOB-BRD 49-19-20	Homogenous	90%	5%	5%	/
MOB-BRD 27-22-16	Homogenous	90%	5%	5%	/
MOB-BRD-27-22-26	Homogenous	70%	25%	/	5%



**Figure 5-15.** Thin section micro-photographs of: **A, B)** ferrous dolomite-akerite in very fine quartz matrix, intersected by a dolomite and red coloured, calcite vein; **C, D)** coarse ferrous dolomite-ankerite as a void-filling.

### 5.2.2. Spilite facies

In the spilite facies, three lithotypes were differentiated based on the difference of the fabric, alteration product, and its intensity – spilite breccia, amygdaloidal basalt, and tuff.

#### 5.2.2.1. Lithotype 4 (LT4): Tuff

The rock appears of pyroclastic origin, as evidenced by the presence of glass shards, plagioclase crystal clasts, and rare biotite crystalloclasts. The matrix consists of very fine-grained quartz, volcanic glass, chlorite, and radiolarians (Table 5-7). The glass shards are needle-like or shaped like the letters V or Y. Tuff has a laminated structure (Fig. 5-16).

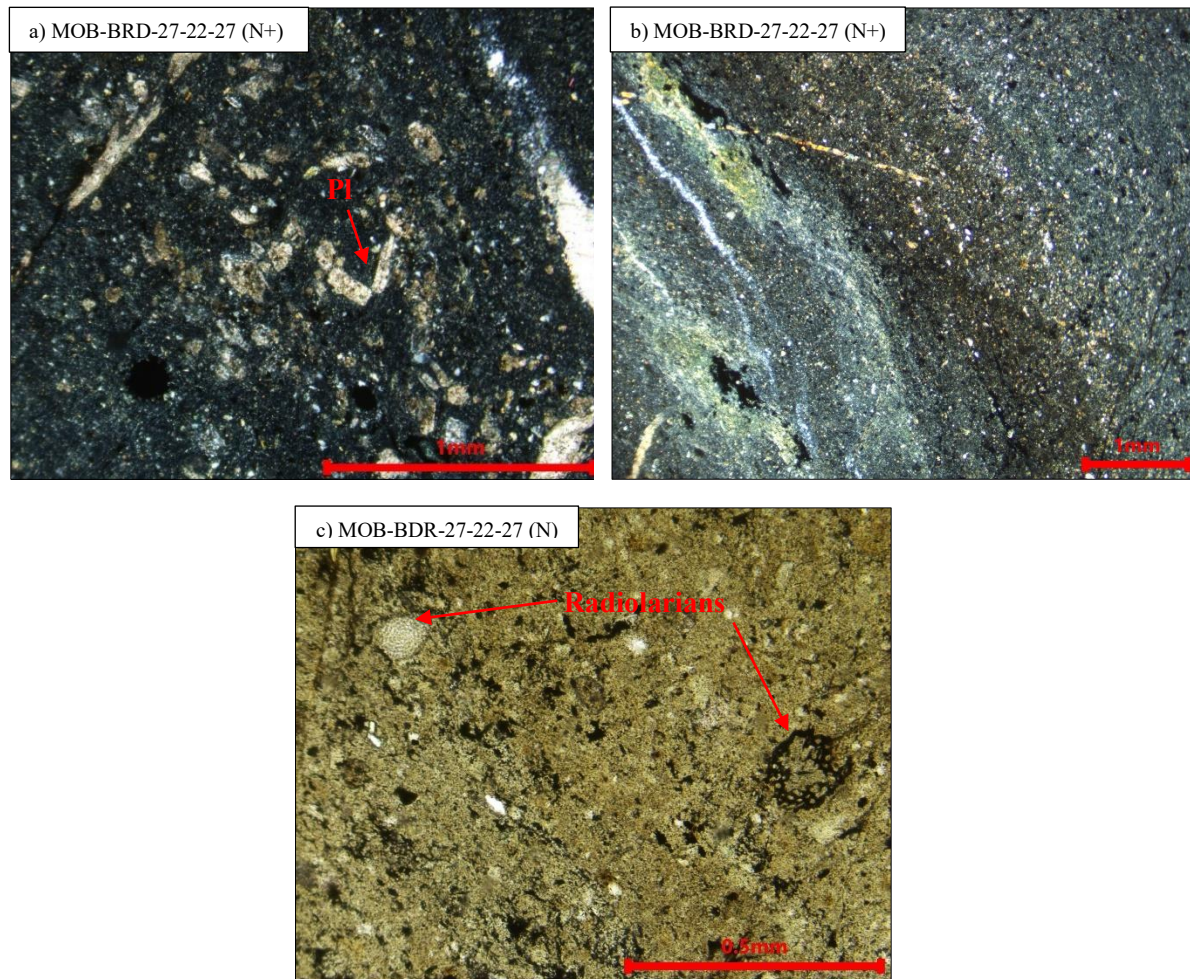
**Plagioclase** crystalloclasts are lamellar, idiomorphic to hypidiomorphic, and subject to common alterations such as carbonatization, sericitization, and albitization. In some crystalloclasts, due to variations in the intensity of alterations, twinning can be recognized. Their size varies from 0,01x0,02 mm to 0,02x0,025 mm. Crystal clasts of **biotite** have a brown



colour and bird-eye extinction. Their size ranges from 0.01 to 0.05 mm. Crystal clasts of **quartz** are prevalent in the matrix. They are primarily fine-grained, irregular in shape, often rounded, and show resorptive edges. Voids are predominantly altered into microcrystalline aggregates of chlorite and Fe-oxides.

**Table 5-7.** Mineral composition of tuff.

Sample	Structure	Mineral composition						
		Quartz	Chlorite	Volcanic glass	Plagioclase	Clay minerals	Calcite	Biotite
MOB-BRD-27-22-27	Laminated	35%	15%	15%	15%	10%	10%	1%



**Figure 5-16.** Thin section micro-photographs of: **A)** sericitized, carbonitized and albitized plagioclase, **B)** laminated tuff structure, **C)** radiolarians sporadically found in the tuff.

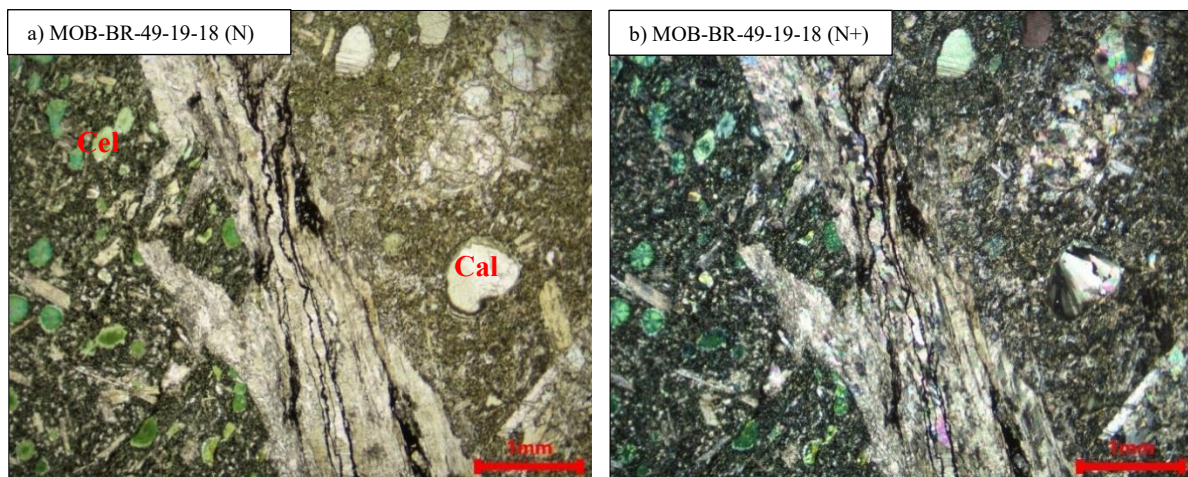
5.2.2.2. *Lithotype 5 (LT5): Amygdaloidal basalt*

The mineral composition of amygdaloidal basalt consists of plagioclase as the main mineral and hematite, chlorite, calcite, albite, and celadonite as secondary minerals. Matrix is composed of very fine argillaceous minerals, Fe-oxides, and chlorite (Table 5-8). The rock structure is amygdaloidal (Fig. 5-17).

**Plagioclase** has tabular, hypidiomorphic habitus, from 0,016x0,024 mm to 0,016x0,16 mm in size. It is colourless to light orange, with polysynthetic twinning and grey interference colour of I. order. It is altered to calcite, chlorite, sericite, and albite. **Celadonite** occurs within interparticle pores, and amygdalas, partially replacing matrix. Bluish-green, fibro-radial, needle-like celadonite show pleochroism and anomalous blue-green interference colour. **Calcite** is present as precipitates within intraparticle spaces, as a vein-filling, as the fibro-radial lining of amygdalas along with celadonite, and as replacing plagioclase. Calcite has a white interference colour of the higher order and rhombohedral cleavage at oblique angles.

**Table 5-8.** Mineral composition of amygdaloidal basalt.

Sample	Structure	Mineral composition					
		Plagioclase	Matrix	Calcite	Chlorite	Celadonite	Hematite
MOB-BR-49-19-18	amygdaloidal	30%	30%	15%	10%	10%	5%
MOB-BR-04-20-02	amygdaloidal	30%	30%	20%	10%	10%	/



**Figure 5-17.** Thin section micro-photographs of: **A)** idiomorphic phenocrysts of plagioclase within very fine argillaceous minerals, calcite, and chlorite. Plagioclase phenocrysts are sericitized and carbonatized; **B)** contact of hematitized and carbonitized amygdaloidal basalt; left side of thin section shows phenocrysts of plagioclase within, mostly hematitized, matrix and celadonite-filling vesicles;

right side of thin section shows phenocrysts of plagioclase within chloritized and celadonized matrix and calcite-filling vesicles.

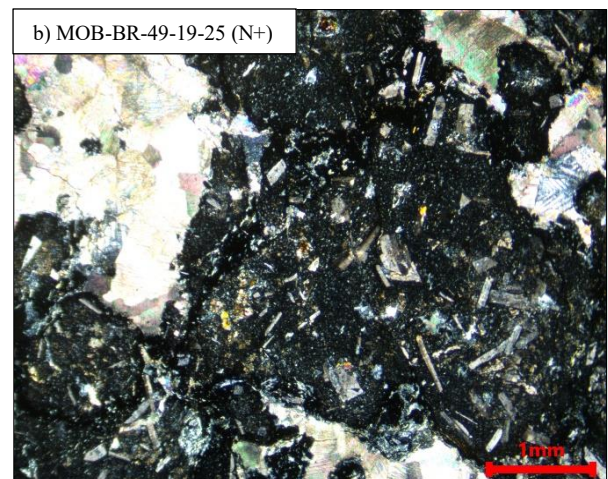
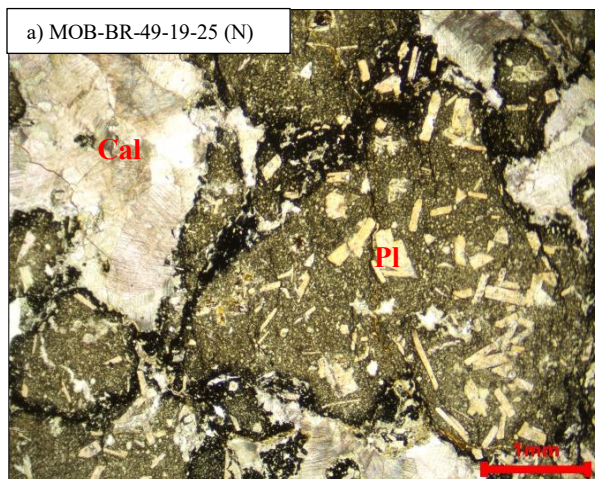
5.2.2.3. *Lithotype 6 (LT6): Spilite breccia*

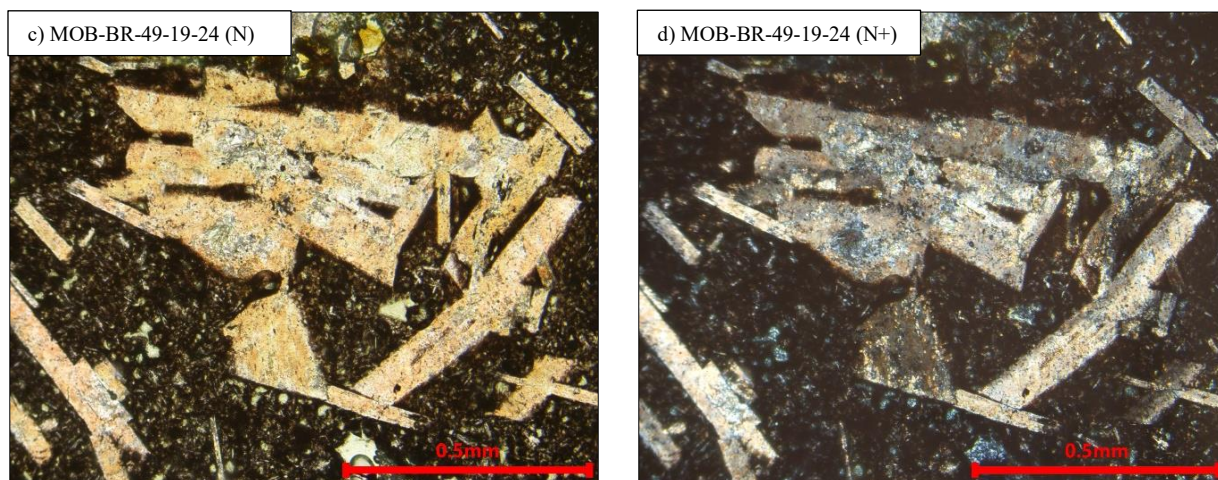
The mineral composition of spilite breccia consists of basalt clasts cemented with calcite and hematite. In the basalt, plagioclase is the primary phase and secondary phases are hematite, chlorite, and calcite. Matrix is composed of very fine argillaceous minerals, hematite, and chlorite (Table 5-9). The rock structure is brecciated (Fig. 5-18. A, B).

**Plagioclase** has lamellar hypidiomorphic to allotriomorphic habitus with polysynthetic twinning and gray interference colour of I. order. It exhibits a light orange colour in PPL (Fig. 5-18. C, D). It is altered to calcite, chlorite, sericite, and albite. Dimensions of phenocrysts vary from 0,018x0,024 mm to 0,5x2 mm. **Calcite** shows interference colour of the higher order and rhombohedral cleavage in XPL. It is present as a plagioclase alteration, amygdaloidal and interstitial filling. **Hematite** is present in the interstitial space as a dark aggregate.

**Table 5-9.** Mineral composition of spilite breccia.

Sample	Structure	Mineral composition				
		Plagioclase	Hematite	Matrix	Calcite	Chlorite
MOB-BR-49-19-24	amygdaloidal	35%	20%	20%	15%	10%
MOB-BR-49-19-25	amygdaloidal	30%	20%	20%	20%	10%





**Figure 5-18.** Thin section micro-photographs of: **A, B)** fragmented spilitic cemented with calcite; **C, D)** idiomorphic phenocrysts of plagioclase within very fine argillaceous minerals, hematite, chlorite. Plagioclase phenocrysts are sericitized, albitized and chloritized.

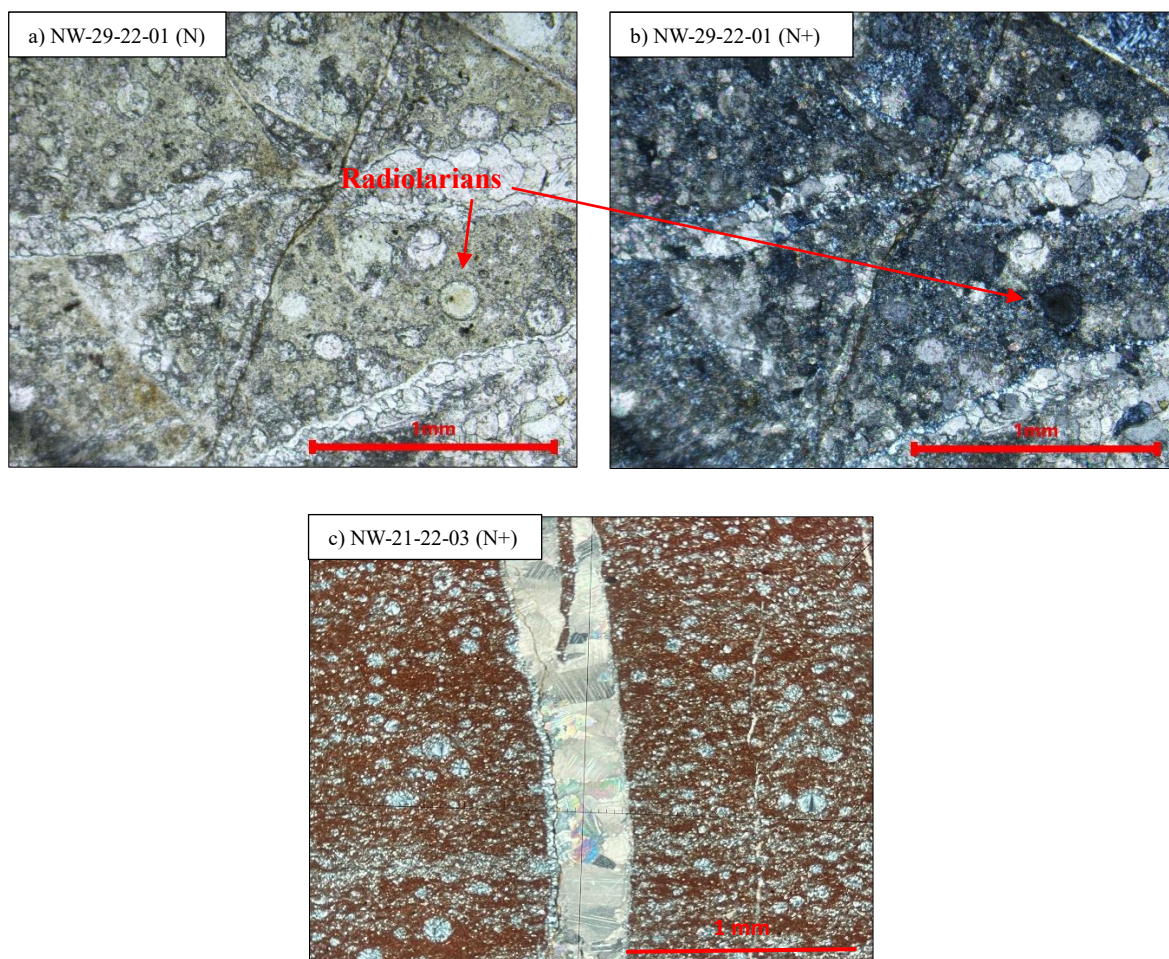
### 5.2.3. Chert facies

#### 5.2.3.1. Lithotype 7 (LT7): Radiolarite

Sample NW-21-22-03 represents the chert with radiolarians displaying an exhaustive red colour produced by hematite aggregates. Radiolarians, filled with chalcedony in radiating and fan-shaped patterns, vary in size from 0.05 to 0.5 mm (Fig. 5-19). The abundance of radiolarians exceeds 15% (Table 5-10). Calcite tension veins intersect the unit. Chalcedony is present at the vein and siltstone contact. In thin section NW-29-22-01, microcrystalline quartz has a uniform mosaic structure, slightly coarser in some areas. It is scattered with calcite grains, and radiolarians are altered to chalcedony rosette. The section is crosscut by calcite and oxidized veins.

**Table 5-10.** Mineral composition of radiolarite.

Sample	Structure	Mineral composition			
		Quartz	Calcite	Chalcedony	Hematite
NW-29-22-01	Homogenous	50%	30%	15%	5%
NW-21-22-03	Homogenous	40%	15%	15%	30%



**Figure 5-19.** Thin section micro-photographs of **A, B)** silicified radiolarians in the; **C)** Hematitized radiolarite.

#### 5.2.4. Ore – bearing facies

##### 5.2.4.1. Lithotype 8 (LT8): Barite-sulphide mineralization

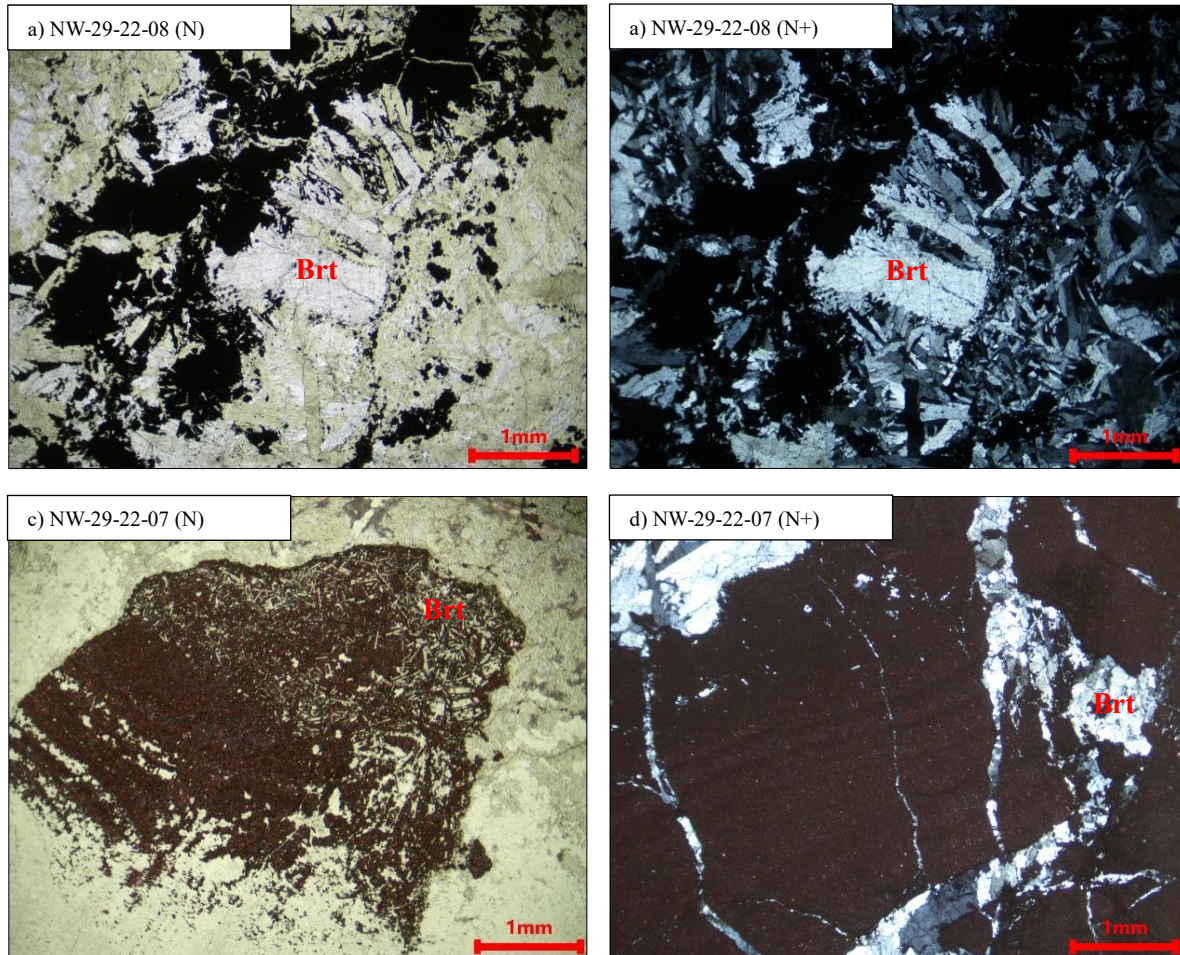
Thin sections from barite-sulphide mineralization are composed of barite and opaque minerals (Table 5-11). Two textures of anisotropic barite are recognized; **Brt1** – coarse-crystalline idiomorphic to allotriomorphic barite, and **Brt2** – vein-filling barite that intersects opaque minerals (Fig. 5-20).

**Brt1** crystals have tabular or needle-like habitus, 0,1x0,3 mm to 0,5x2 mm in size. In PPL, it is colourless, and in XPL, it shows grey and white interference colour of I. order, pleochroism, and parallel extinction. **Brt2** is fine-crystalline in dimensions and has allotriomorphic habitus.

**Table 5-11.** Mineral composition of barite-sulphide mineralization.

Sample	Structure	Mineral composition	
		Barite	+/- Pyrite, marcasite, sphalerite, galena, tetrahedrite

NW-29-22-07	Massive	30%	70%
NW-29-22-08	Massive	75%	25%



**Figure 5-20.** Thin section micro-photographs of: **A, B)** opaque minerals crystallized in the interstitial space around idiomorphic barite, **C, D)** barite overprinting sulphide minerals.

#### 5.2.4.2. Lithotype 9 (LT9): Mineralized dolomite breccia

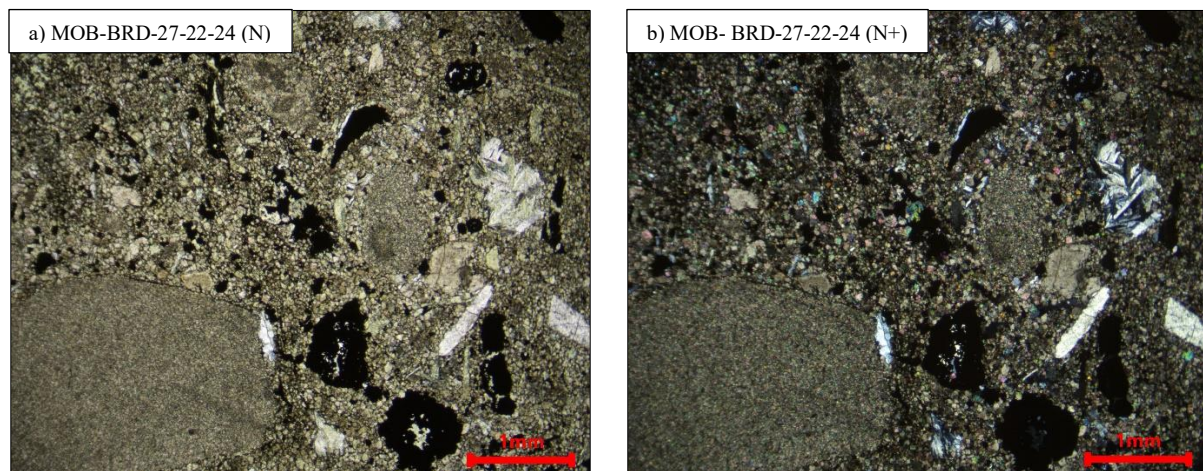
In the sample MOB-BRD-27-22-24, the matrix, accounting for about 80% of the breccia, is mainly composed of Fe-dolomite-ankerite, barite, and opaque minerals. Dolostone fragments form a minor phase (Table 5-12; Fig. 5-14). It is affected by secondary silicification and dolomitization as the void-filling.

**Non-ferrous dolomite (Dol1)** crystals are colourless and have idiomorphic to allotriomorphic rhombohedral habitus. **Ferrous dolomite-ankerite (Dol2)** is similar to dolomite in thin sections but stained brown by iron oxidation. The interference colours both have white of the higher order. The crystal size of Dol1 is around 0,0025x0,003 mm. Dimensions of Dol2 crystals are approximately 0,015x0,02 mm. **Barite** crystals are typically tabular or often intergrown,

forming rosettes or concretionary masses with a fibrous texture. In PPL, it is colourless, and in XPL, it shows gray and white interference colour of I. order and parallel extinction. Crystal dimension exhibits from 0,008x0,032 mm to 0,08x0,576 mm.

**Table 5-12.** Mineral composition of mineralized dolomite breccia.

Sample	Structure	Mineral composition				
		Fe-dolomite-an-kerite	Dolomite	Quartz	Barite	Galena, spfalerite
MOB-BRD-27-22-24	Breccia	30%	25%	20%	15%	10%



**Figure 5-14.** Thin section micro-photographs of hypidiomorphic opaque ore minerals and the idiomorphic tabular and rozzete-like barite grains within Fe-dolomite-ankerite cement of the dolomitic breccia.

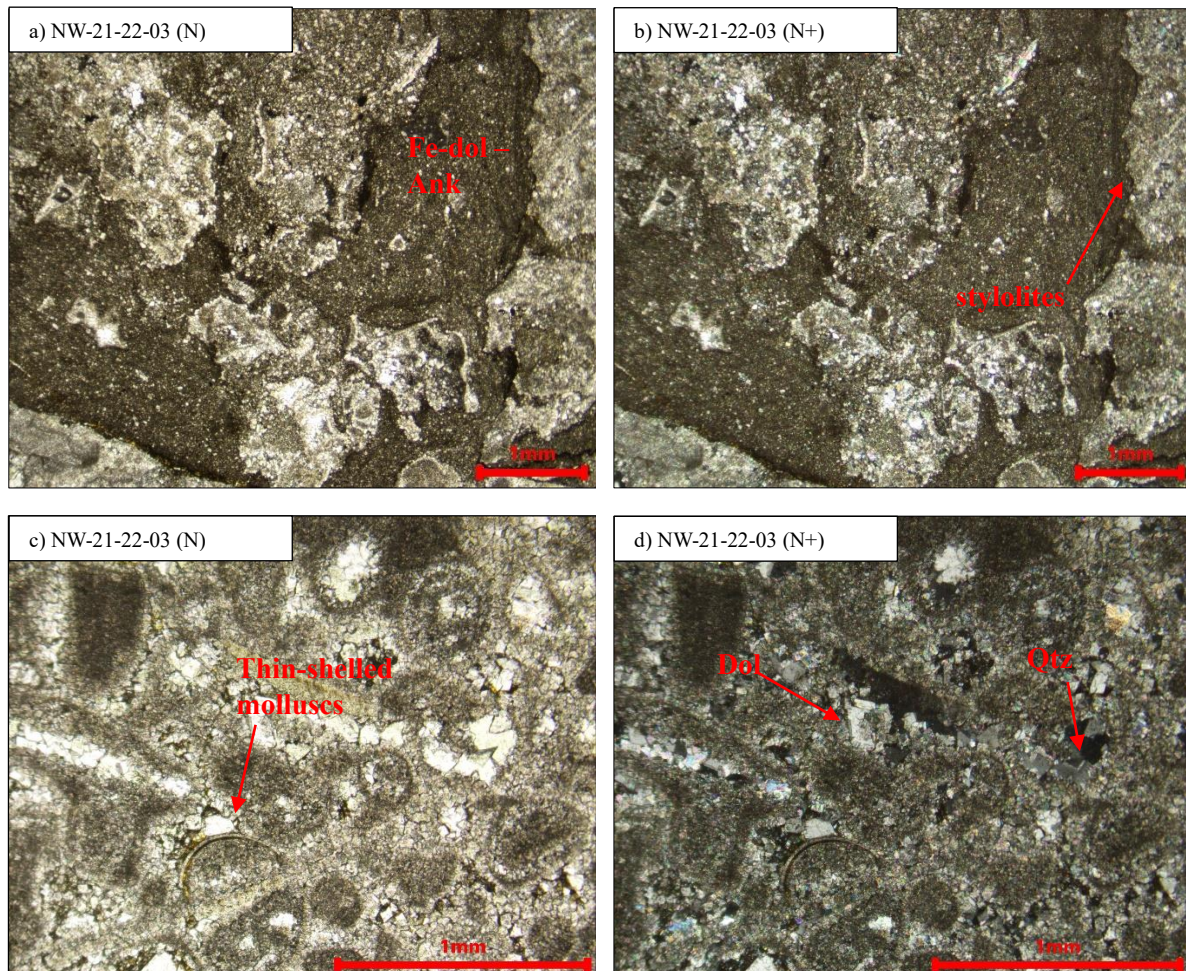
### 5.2.5. Dolomite breccia facies

#### 5.2.5.1. Lithotype 10 (LT10): Dolomite breccia

A thin section of sample NW-21-22-02 contains angular fragments of dolostone with bioclastic packstone fabric, recrystallized gastropods, and thin-shelled molluscs within a Fe-dolomite-ankerite cement (Table 5-13). About 60% of the sample consists of dolostone fragments, indicating that the cement is a minor phase. Suture and sharp peak stylolites between the fragments and the cement are present in the thin section shown in Fig. 5-22. A, B. Dolostone is partially dolomitized and silicified (Fig. 5-22. C, D). Determined textural types of carbonate minerals are Dol1- a main mineral component of the dolostone fragments; Dol2- a Fe-dolomite-ankerite cement; and void-filling.

**Table 5-13.** Mineral composition of dolomite breccia.

Sample	Structure	Mineral composition		
		Dolomite	Fe-dolomite-ankerite	Quartz
NW-21-22-02	dolomitic breccia	55%	40%	5%



**Figure 5-22.** Thin section micro-photographs of NW-21-22-02 sample: **A, B**) angular, non-ferrous dolostone fragments within ferrous dolomite-ankerite matrix, **C**) thin-shelled molluscs, **D**) partly dolomitized and silicified dolostone fragments.

### 5.2.6. Limestone facies

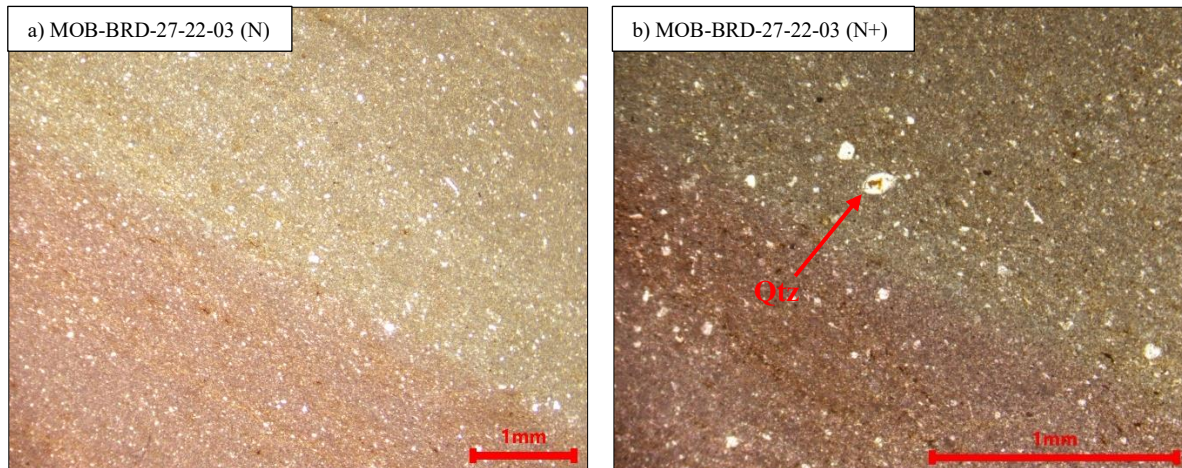
#### 5.2.6.1. Lithotype 11 (LT11): Mudstone lithotype

In the mudstone composition, the dominant phase is red-coloured calcite mud, while quartz and hematite form a minor phase (Table 5-14; Fig. 5-23). The laminated structure sporadically contains rounded limestone fragments.



**Table 5-14.** Mineral composition of mudstone.

Sample	Structure	Mineral composition		
		Calcite	Quartz	Hematite
MOB-BRD-27-22-03	Laminated	80%	10%	10%

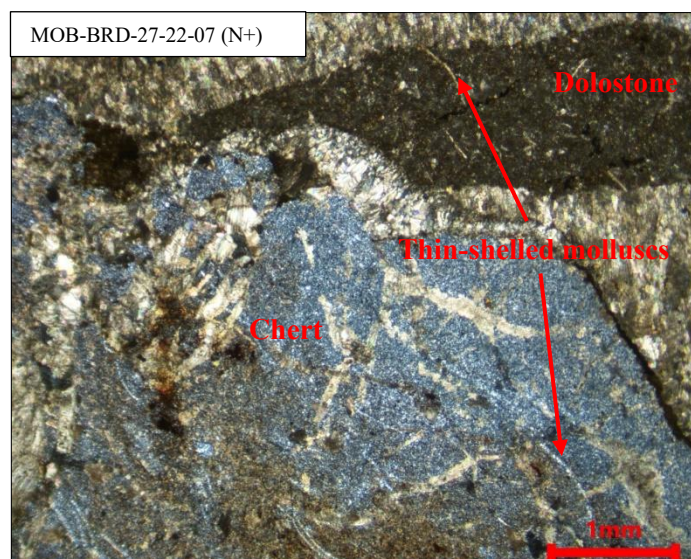


**Figure 5-23.** Thin section micro-photographs of red-coloured clayey mudstone with coarse quartz.

#### 5.2.7. Contact zones

##### 5.2.7.1. Contact of dolostone and radiolarite lithotype

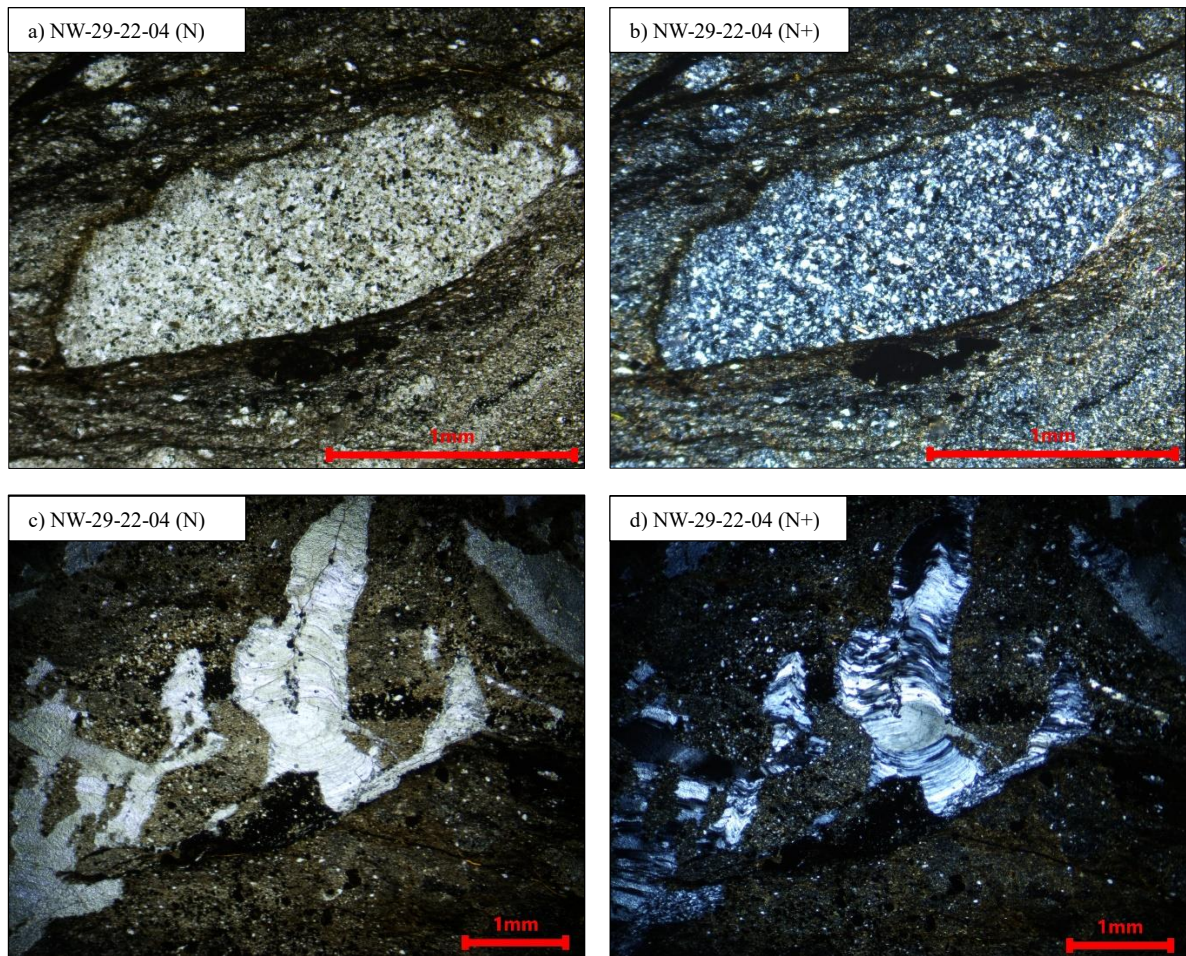
Thin section MOB-BRD-27-22-07 presents dolostone and radiolarite contact with thin-shelled molluscs deposited in both lithologies (Fig. 5-24). At the contact of the rocks is oxidized calcite vein.



**Figure 5-24.** Thin section micro-photographs of a contact zone of deep marine chert and dolostone intersect with oxidized veins.

#### 5.2.7.2. Contact of siltstone and marl lithotype

NW-29-22-04 consists of the silty mass where coarse-crystalline barite and fragments of pyroclastic rock are embedded. In the matrix, white mica, dolomite, and quartz are recognized. It gradually changes its composition to fine-grained marl. Barite undergoes ductile deformation during vein filling, supported by a rotation of pyroclastic fragments and oxidized shear bands that define wavy foliation (Fig. 5-15. A, B).



**Figure 5-15.** A, B) Thin section micro-photographs of pyroclastic fragments within siltstone indicating pyroclastic re-work; C, D) ductile deformation of the barite-filled vein.

### 5.3. X-ray diffraction analysis

Eleven samples were analyzed by XRD method: MOB-BR-49-19-18, MOB-BR-49-19-20, MOB-BR-49-19-24, MOB-BR-49-19-25, MOB-BRD-27-22-10, MOB-BRD-27-22-14, MOB-BRD-27-22-15, MOB-BRD-27-22-16, MOB-BRD-27-22-24, NW-29-22-04, and NW-11-22-08 (Table 5-15). These samples were chosen based on prior micropetrographic analyses.

MOB-BR-49-19-18's XRD image indicates plagioclase is the dominant mineral phase, while chlorite and hematite are in minor amounts.

Distinguishing between non-ferrous dolomite and ferrous dolomite-ankerite based on their XRD patterns can be challenging as they tend to overlap. In the case of sample MOB-BR-49-19-20, XRD analysis indicates the presence of ankerite, but it will be interpreted as Fe-dolomite-ankerite. Sample MOB-BRD-27-22-24 primarily comprises Fe-dolomite-ankerite and barite as the dominant minerals.

Spilite samples MOB-BR-49-19-24 and MOB-BR-49-19-25 consist primarily of plagioclase and quartz, with secondary minerals such as hematite, chlorite, calcite, illite +/- ilmenite and dolomite. MOB-BRD-27-22-15 and MOB-BRD-27-22-16 are primarily composed of quartz and dolomite. MOB-BRD-27-22-15 also contains small amounts of pyrite, while MOB-BRD-27-22-14 and MOB-BRD-27-22-16 contain anatase. Sample NW-29-22-07 exhibits ore - bearing minerals – barite, pyrite, and marcasite, while NW-29-22-08 includes mainly barite, and sfalerite+galena+tetrahedrite in minor amounts. Lastly, sample NW-11-22-08 is composed of quartz and pyrite, with occasional traces of galena.

**Table 5-15.** XRD analysis results.

Sample ID	Determination	Quartz	Dolomite	Calcite	7Å	10Å	14Å	Illite	Barite	Other minerals
BRD 11-22-08	Silicified marl	+++				+		?		Galena, pyrite
BRD 27-22-10	Dolomitic siltstone	++			?	++	?	?		Sphalerite
BRD 27-22-15		++	++			++		?		Pyrite
BRD 27-22-14	Silicified siltstone	+++	?			++		?		Anatase, hematite
BRD 29-22-04		++				++			+++	Kuramite, microcline
BRD 49-19-18	Amygdaloidal basalt	?		++	?	+	++	+		Chlorite/vermiculite, plagioclase (major phase), hematite
BRD 49-19-24	Spilite breccia	+		++	?	+	+	?		Plagioclase (major phase), hematite
BRD 49-19-25		+	+	++	?	+	+	+		Chlorite/vermiculite, plagioclase (major phase), hematite and/or ilmenite
BRD 27-22-16	LD dolomite	++	++			++				Anatase
BRD 49-19-20		+		+	?	+	?			Ankerite (major phase)
BRD 27-22-24	Mineralized breccia	?	+++			+			+	Barite
NW-29-22-07	Massive mineralization								+	Barite, pyrite, marcasite
NW-29-22-08									++	Barite, sfalerite, galena, tetrahedrite

## 5.4. X-ray fluorescence analysis

The results of XRF analysis of samples are presented in Tables 5-16 and 5-17. The content of major elements is displayed in mass percentages of oxides (Table 5-16), while trace elements are shown in parts per million (ppm) units (Table 5-17).

### 5.4.1. Major elements

The analyzed rocks exhibit a wide range of **SiO<sub>2</sub>** content, varying from 5 to 95 mass %. The SiO<sub>2</sub> values are observed in the mineralized zone, dolomitic breccia, and massive LD dolomite. Amygdaloidal basalt and spilitic breccia have comparable SiO<sub>2</sub> values (70.26-75.26 mass %). Siltstone and marl exhibit SiO<sub>2</sub> concentrations slightly higher at approximately 65 mass %. However, when in contact with the mineralized zone due to the alteration halo, the concentration of SiO<sub>2</sub> significantly increases and reaches values between 81-95 mass %.

The concentration of **TiO<sub>2</sub>** in most samples is up to 0.65 mass %. However, some samples like LD dolomite (27-22-16), amygdale basalt (MOB-BR-49-19-18), spilitic breccia (MOB-BR-49-19-25), and mineralized breccia (MOB-BRD-24-22-24) have values ranging from 1.18-3.34 mass %, with sample MOB-BR-49-19-20 having the highest concentration of 7.19 mass %.

The concentration of **Cr<sub>2</sub>O<sub>3</sub>** is up to 0.65 mass % in all analyzed samples.

The **Al<sub>2</sub>O<sub>3</sub>** concentration in the analyzed samples ranges from 1.93 mass % to 21.45 mass %. Samples of dolomitic breccia (NW-21-22-02), silicified marl (NW-11-22-08), LD dolomite (MOB-BR-49-19-20), and mineralized breccia (MOB-BRD-27-22-24) have the lowest values (1.93-7.14 mass %). The medium value (14.34-15.82 mass %) is found in samples of silicified siltstone (NW-29-22-04), and LD dolomite (MOB-BRD-27-22-16). The highest values (18.12-21.45 mass %) are found in samples of spilitic breccia (MOB-BR-49-19-24, MOB-BR-49-19-25), amygdaloidal basalt (MOB-BR-49-19-18), silicified siltstone (MOB-BRD-27-22-14), dolomitic siltstone (MOB-BRD-27-22-10 and MOB-BRD-27-22-15).

**Fe<sub>2</sub>O<sub>3</sub>** in most samples varies in concentration up to 2.67 mass %.

The concentration of **MnO** in analyzed samples is approximately 0.03 mass %

The **MgO** content in the analyzed samples ranges from 0.41 mass % to 73.08 mass %. Samples of silicified marl (NW-11-22-08), silicified siltstone (MOB-BRD-27-22-14 and NW-29-22-04), samples of spilitic breccia (MOB-BR-49-19-24 and MOB-BR-49-19-25), and amygdale basalt (MOB-BR-49-19-18) have the lowest concentration (0.41-6.81 mass %). The medium

values (12.11-25.35 mass%) are found in dolomitic siltstone (MOB-BRD-27-22-15), LD dolomite (MOB-BRD-27-22-16), and dolomitic breccia (NW-21-22-02). The highest values are found in LD dolomite MOB-BR-49-19-20 (56.62%) and mineralized breccia MOB-BRD-27-22-24 (73.08 mass %).

The **CaO** concentrations in most samples is approximately 1.87 mass %, while in the sample of dolomitic breccia, it is 57.27 mass %.

The **K<sub>2</sub>O** content reach up to 1%.

Since the XRF method cannot calculate the concentration of CO<sub>2</sub>, the concentration of CaCO<sub>3</sub>, i.e., CaO, cannot accurately reflect its actual values. Therefore, the concentrations of other oxides in the samples are also not accurate.

**Table 5-16.** Results of XRF analysis (%).

Sample	Determination	SiO <sub>2</sub>	TiO <sub>2</sub>	Cr <sub>2</sub> O <sub>3</sub>	Al <sub>2</sub> O <sub>3</sub>	Fe <sub>2</sub> O <sub>3</sub>	MnO	MgO	CaO	K <sub>2</sub> O
NW-11-22-08	Silicified marl	95	0.02	BDL	4.34	0.24	BDL	0.41	BDL	BDL
MOB-BRD-27-22-10	Dolomitic siltstone	68.24	0.17	0.01	21.28	0.06	BDL	9.37	BDL	0.88
MOB-BRD-27-22-15		65.22	0.43	BDL	21.45	BDL	BDL	12.11	BDL	0.7
MOB-BRD-27-22-14	Silicified siltstone	74.35	0.72	BDL	20.68	1.3	BDL	2.41	BDL	0.67
NW-29-22-04		81.04	0.65	BDL	14.34	0.01	BDL	2.67	1.3	BDL
MOB-BR-49-19-18	Amygdaloidal basalt	70.85	2.63	BDL	19.18	0.01	0.02	6.28	BDL	1.03
MOB-BR-49-19-24	Spilitic breccia	75.26	0.66	0.02	18.12	0.38	0.02	4.95	BDL	0.94
MOB-BR-49-19-25		70.56	3.34	BDL	18.32	BDL	0.03	6.81	BDL	0.95
MOB-BRD-27-22-16	LD dolomite	62.12	1.18	BDL	15.82	BDL	BDL	20.4	BDL	0.48
MOB-BR-49-19-20		28.42	7.19	0.02	6.99	BDL	0.02	56.62	0.75	BDL
NW-21-22-02	Dolomitic breccia	9.8	0.01	0.05	3.08	2.67	1.32	25.35	57.27	0.7
MOB-BRD-27-22-24	Mineralized breccia	15.25	3.15	BDL	7.14	0.38	0.02	73.08	1.02	BDL

#### 5.4.2. Trace elements

The highest concentration of Ba, Zn, and Pb elements is present in samples of mineralized breccia (MOB-BRD-27-22-24), followed by silicified siltstones (MOB-BRD-27-22-14, NW-29-22-04) and marls (NW-11-22-08). The occurrence of ore minerals such as barite, galena, and sphalerite can explain these concentrations. Sr has an elevated concentration in silicified marls, siltstones, and mineralized dolomitic breccia, probably as a consequence of substituting Ca with Sr. Cu is almost negligible, except in the sample of spilitic breccia MOB-BR-49-19-24, where it is 11 ppm. The concentration of P in spilitic breccia and amygdaloidal

basalt is elevated (1085-1289 ppm). Samples of LD dolomite (MOB-BRD-27-22-16), silicified siltstone (MOB-BRD-27-22-14), and dolomitic marl (MOB-BRD-27-22-10, MOB-BRD-27-22-15) exhibit concentrations of Ag from 11 ppm to 23 ppm.

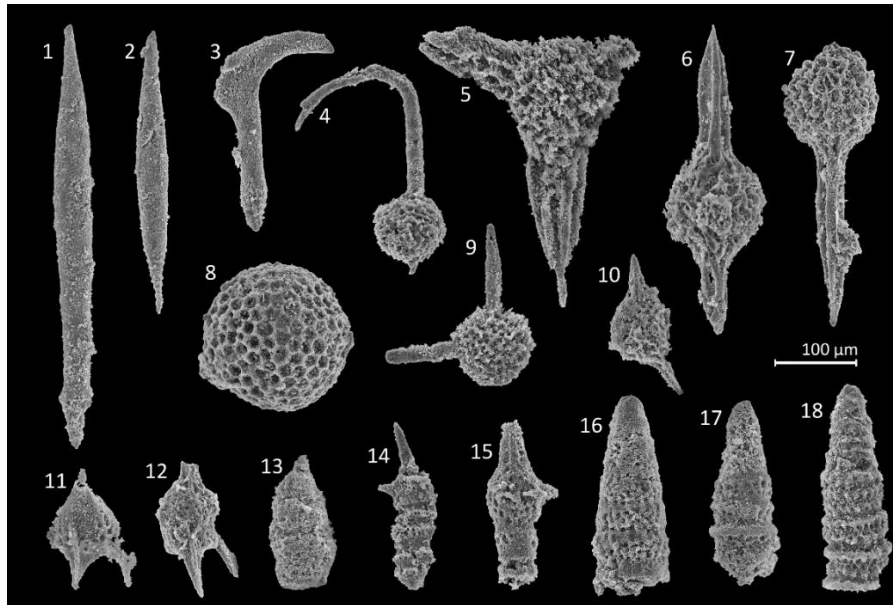
**Table 5-17.** Results of XRF analysis (ppm).

Sample	NW-11-22-08	MOB-BRD-27-22-10	MOB-BRD-27-22-15	MOB-BRD-27-22-14	NW-29-22-04	MOB-BR-49-19-18	MOB-BR-49-19-24	MOB-BR-49-19-25	MOB-BR-49-19-20	MOB-BRD-27-22-16	MOB-BRD-27-22-24
Determination	Silicified marl	Dolomitic marl		Silicified siltstone		Amygdaloidal basalt	Spilite breccia		LD dolomite		Mineralized dolomitic breccia
<b>Rb</b>	BDL	BDL	BDL	BDL	275	BDL	BDL	158	BDL	BDL	185
<b>Sr</b>	309	44	76	615	BDL	47	40	96	74	58	441
<b>Ba</b>	486	BDL	BDL	301	61991	BDL	BDL	BDL	270	BDL	6753
<b>Cu</b>	BDL	BDL	BDL	BDL	BDL	BDL	3	BDL	BDL	BDL	BDL
<b>Ag</b>	BDL	14	15	12	BDL	BDL	BDL	BDL	BDL	11	23
<b>Zn</b>	33	164	103	166	97	81	147	160	31	81	21
<b>Pb</b>	3976	48	18	54	19165	57	81	65	58	34	1426
<b>Cd</b>	10	BDL	BDL	BDL	13	BDL	BDL	BDL	BDL	BDL	11
<b>P</b>	BDL	887	700	248	BDL	1085	1289	742	687	612	BDL
<b>As</b>	BDL	BDL	22	BDL	BDL	23	21	BDL	BDL	BDL	BDL
<b>S</b>	75169	BDL	BDL	9597	158052	BDL	BDL	BDL	BDL	5421	51362

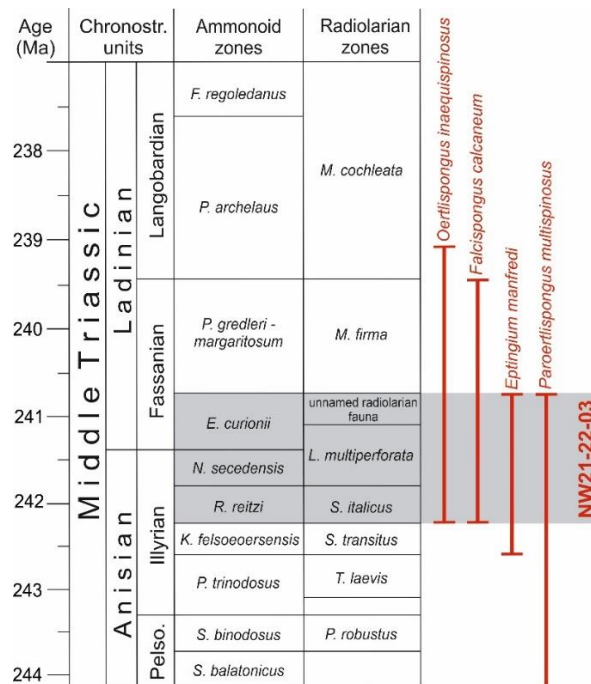
## 5.5. Fossils age determination

### 5.5.1. Radiolarian dating

Radiolarians are present in samples NW-21-22-03, NW-29-22-01 and MOB-BRD-27-22-27. In total, 18 radiolarian species were determined in the sample, of which 10 are open for nomenclature. Identified radiolarians are shown in Fig. 5-17. The stratigraphic ranges of selected species are shown in Fig. 5-16.



**Figure 5-16.** Middle Triassic radiolarians from sample NW21-22-03: 1) *Paroertlispongos multispinosus* Kozur and Mostler; 2) *Paroertlispongos* ? sp. 1 sensu Dumitrica (1999); 3) *Falcispongos calcaneum* Dumitrica; 4) *Oertlispongos inaequispinosus* Dumitrica, Kozur and Mostler; 5) *Eptingium manfredi* Dumitrica; 6) *Pseudostylosphaera timorensis* Sashida and Kamata; 7) *Pseudostylosphaera longispinosa* Kozur and Mostler; 8) *Archaeocenosphaera* sp.; 9) *Tetrapaurinella* ? sp.; 10) *Cryptostephanidium* sp. cf. *cornigerum* Dumitrica 11) *Eonapora* ? sp.; 12) *Hozmadia* sp. cf. *H. reticulata* Dumitrica, Kozur and Mostler; 13) *Conospongocyrtis* ? sp.; 14) *Turrinasus* ? sp.; 15) *Komospinocyrtis anisica* (Kozur and Mostler); 16) *Triassocampe* sp.; 17) *Triassocampe* sp. cf. *T. deweveri* (Nakaseko and Nishimura); 18) *Triassocampe scalaris* Dumitrica, Kozur and Mostler.



**Figure 5-17.** Stratigraphic ranges of selected radiolarian species determined in sample NW21-23-03 (range of *O. inaequispinosus* according to Stockar et al. (2012) and Ozsvárt et al. (2023); other ranges

from Stockar et al. (2012). Middle Anisian to Ladinian radiolarian zones tied to ammonoid zones adopted from Kozur (2003). Numerical ages are given according to Ogg and Chen (2020).

### 5.5.2. Foraminifera dating

Benthic foraminifera are determined in the dolomitic marl sample (MOB-BR-49-19-11). Species *Meandrospira dinarica* Kochansky-Devidé and Pantić is differentiated. This species is well known from the Middle Triassic strata of the Dinarides (e.g., Goričan et al., 2005; Kukoč et al., 2023). It appears at the base of the Anisian and ranges until early Illyrian (Kukoč et al., 2023).

## 6. DISCUSSION

### 6.1. Interpretation of depositional conditions and environment of facies

The area of the Rupice deposit is highly tectonically disturbed, so most facies are in tectonic contact, making it challenging to track stratigraphic changes and depositional conditions of individual units within a single column. However, lithotypes remain undisturbed, enabling the monitoring of changes in petrological properties and depositional conditions within facies.

#### 6.1.1. Footwall host rocks – Siliciclastic-carbonate facies (LT1A, LT2A, LT3)

Anisian siliciclastic-carbonate facies found above the Anisian-Ladinian units, indicate that this facies has been thrust onto the radiolarite and mineralization zone by reverse faulting.

Paragenesis of **dolomitic marl (LT1A)** includes dolomite, quartz, and white mica. The presence of small benthic foraminifera in the marly sediment indicates a pelagic marine environment. It gradually changes composition to fine-grained siltite, indicating they are in stratigraphic contact. Sandstone lenses, fragments of limestone, and pyroclastic rocks embedded in **dolomitic siltstone (LT2A)**, and the stress patterns observed around limestone fragments indicate deposition from gravitational currents. The gradual transition from siltstone to **dolomicrite (LT3A)** suggests a reduction in siliciclastic input and the deposition of carbonate. **Late diagenetic dolomite (LT3B)** is present in dolomites in contact with the mineralization zone and volcanic rocks. Dolomitization models are described in 6.2.

#### 6.1.2. Hanging wall – radiolarite (LT7)

The presence of the Anisian-Ladinian radiolarians indicates deposition in deep marine conditions. Secondary silicification and hematitization suggest an input by hydrothermal fluid



enriched with silica and iron (distal hydrothermal source?). The contact between radiolarite and massive mineralization is tectonic, and presumed to have formed after mineralization, so the age of the MOB may be limited to the Middle Triassic.

### 6.1.3. Magmatic-hydrothermal event

#### 6.1.3.1. *Silicified marl and siltstone (LT1B, LT2B)*

At the contact with the mineralization zone, **marl (LT1B)** and **siltite (LT2B)** have undergone silicification, and sericitization associated with the growth of framboidal pyrite. Silicification and sericitization can be interpreted as an alteration halos around the deposit, reflecting the system's interaction with surrounding rocks and sediments, resulting in chemical and mineralogical changes. Nevertheless, it's important to consider that the mineral assemblages and geochemical zoning do not exclusively originate from the hydrothermal metasomatism linked to the mineralizing event. Instead, they emerge as a result of the combined influences of the original rock composition and various processes that have altered it (Madeisky and Stanley, 1993). Based on the stress patterns observed around barite clasts and tuff fragments in siltite (LT2B), it can be concluded that the material was, in the post-mineralization stage, under the influence of the tectonic activity.

#### 6.1.3.2. *Dolomitic breccia facies (LT10)*

The dolomitic breccia consists of angular clasts of partly silicified and dolomitized dolostone. Gastropods and thin-shelled molluscs found in clasts are indicators of the deposition of source rock in a pelagic marine environment. Given the unsorted nature of the dolostone fragments, it is possible that the unit was deposited by tectonic fragmentation of Lower Triassic and Paleozoic rocks due to advanced rifting. The presence of ferrous dolomite-ankerite cement suggests a possible hydrothermal origin of the cementation event.

#### 6.1.3.3. *Spilite facies*

Considering that only fragmented hematitized basalt is found in the **spilite breccia (LT6)**, it can be concluded that the magma erupted on the surface of the seafloor without causing its fragmentation but inducing diagenetic change. The spilite breccia formed syn-eruptively when the magma encountered seawater, rapidly cooling and solidifying to produce sharp and irregular-edged fragments in the processes of autofragmentation (McPhie et al., 1993). The clasts were later cemented with calcite, and celadonite and rhodochrosite in minor concentration.

**Amygdaloidal basalt (LT5)** exhibits vesicular texture without fragmentation, attributed to slower crystallization without volume reduction. Amygdales are present in a high concentration, with regular and rounded shapes, suggesting their formation by releasing previously trapped volatiles.

The appearance of glass shards (V- and Y- shaped) in tuffs, as well as amygdaloids in basalt indicates a significant amount of volatiles in the volcanic system. The laminated structure of **tuffs (LT4)**, suggests that the pyroclastic material was transported by tractive transport to the deposition site. The tuffs were subsequently re-worked, as evidenced by pyroclastic fragments in the siltstone. Layers of chert and the presence of radiolarians in the tuffs suggest deposition in deep sea conditions with an increased SiO<sub>2</sub> component, derived from pyroclastic material or distal submarine hydrothermal vents. During the Middle Triassic period, there was evidence of magmatic activity and volcanism in the Central Dinarides linked to the emergence of the oceanic Dinaridic Tethys (Trubelja et. al., 2004). The discovery of Anisian-Ladinian radiolarians in the laminate tuff further suggests a correlation between magmatic events in the Rupice region and those in other parts of the Central Dinarides.

#### 6.1.3.4. *Ore – bearing facies*

Two types of barite texture are present in the mineralized zone, indicating polygenetic mineralization. The first type is coarse-crystalline, tabular, hypidiomorphic to idiomorphic barite (Brt1), while the second type is baritic veins (Brt2) that intersect opaque minerals. Ore-bearing zone displays broad zonation, ranging from copper-gold-rich mineralization in the center to distal barite-silver-lead-zinc. Metal zonation on a local scale is complex due to repeated overprinting and structural deformation (Vujević, 2023).

#### 6.1.4. Limestone facies (LT11)

Considering the major presence of calcite and the absence of marine fossils and dolomite, which predominantly form the stratigraphically older facies, it can be inferred that the depositional conditions in the mudstone lithotype are different. It is caused by the cessation of magnesium input, leading to the deposition of calcitic material, likely in a shallower marine environment. Weathering products are differentiated such as hematite and limonite.

## 6.2. Alterations

### 6.2.1. Mechanism of dolomitization

Two types of late-diagenetic dolomites were differentiated in the investigated rock types:

- i) Replacive, non-ferrous dolomite (Dol1), and
- ii) Ferrous dolomite that occurs as pore space-filling (Dol2).

The petrographic features suggest polygenetic dolomitization of studied dolomite rocks. Both types of LD dolomite are in contact with volcanogenic and massive ore-bearing zone, so their formation can be explained with two dolomitization models.

**The dolomitization model by seawater** emphasizes that seawater can cause dolomitization if there is a sufficient mechanism for water percolation through carbonate sediment. The driving mechanism of seawater circulation through extreme parts of platforms can be ocean currents and oceanic changes, the subsidence of more saline water from the surface of the platform downwards, and thermal convection caused by the circulation of elevated-temperature water from the volcanic subsurface. Thermal convection flow may be responsible for the dissolution of carbonates and the formation of massive dolomites that replace them (Flügel, 2004). The observed idiomorphic to hypidiomorphic, rhombohedral, coarse Dol1 likely belongs to this model due to its contact with the spilite unit.

Formation of ferrous-dolomite-ankerite (Dol2) that may be influenced by hydrothermal events. It crystallized in the voids and microcracks as coarse grains with undulatory extinction. It can be explained with a model of **the dolomitization under burial conditions**. Sources of Mg include pressure dissolution and the circulation of hydrothermal solutions (Flügel, 2004, and associated references). The criterion for recognizing dolomitization under burial conditions is the occurrence of large dolomite crystals, saddle dolomite, elevated iron content in dolomite, syngenetic, or earlier formation of dolomite together with stylolites (Flügel, 2004).

### 6.2.2. Spilite alterations

Chlorite is present in the volcanoclastic facies as a secondary mineral crystallized at the expense of volcanic glass, biotite, plagioclase, and other mafic minerals. Plagioclase exhibits chloritization, sericitization and albitization. Spilite breccia has predominately hematitized matrix, indicating an oxidized environment during the period of deposition and early

diagenesis. The oxidized conditions were probably determined by the high content of dissolved oxygen in the bottom water (Li et al., 2011). Celadonite and calcite were formed in the post-mineralization stage from the low-temperature hydrothermal fluid.

#### 6.2.3. Silicification and sericitization

The silicification and sericitization impacts nearly all rock types, except limestone, to various extents. Rocks in proximity to mineralization tend to experience a higher degree of alterations. Such findings imply that the fluid accountable for the alterations may be linked to the ore hydrothermal stage so that the alterations can be interpreted as halos around the mineralized area.

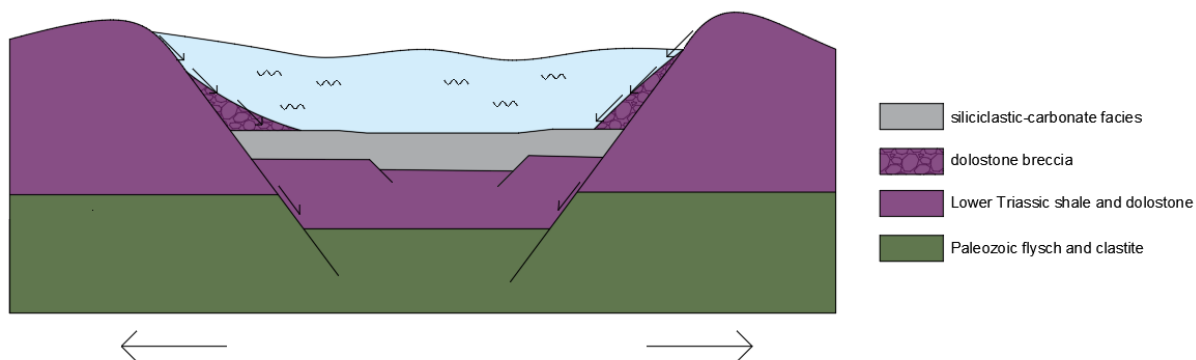
#### 6.2.4. Framboidal pyrite

Framboidal pyrite appears in silicified marl and siltstone associated with quartz and sericite. Apart from marl and siltstone, it is present in massive barite in different ordering stages, from completely disorganized to fully spherical framboids, according to Vujević (2023). Framboidal pyrite has a hypidiomorphic, pyritohedral habitus and does not show signs of deformation due to host rock foliation, suggesting that it was grown in the post-mineralization phase. The occurrence of framboidal pyrite is common in marine sediments, organic matter-bearing sedimentary rocks, and it has also been reported from many sedimentary ore deposits, e.g. sedimentary-exhalative (SEDEX), volcanogenic massive sulphide (VMS), Irish, and sediment-hosted copper, but they are absent in some others (e.g., typical orogenic related Mississippi Valley Type, MVT) (A. Rajabi, 2018).

### **6.3. Genesis of the Rupice deposit**

#### 6.3.1. The first phase: Anisian

In the Anisian, basin opening began along with the deposition of the oldest member—the carbonate-silicate facies (Fig. 6-1). It consists of interbedded silty dolomicrite, siltite and marl, with significant siliciclastic input from the land. Since there are no coarse clastic materials, the Rupice is located in a distal part of the basin.

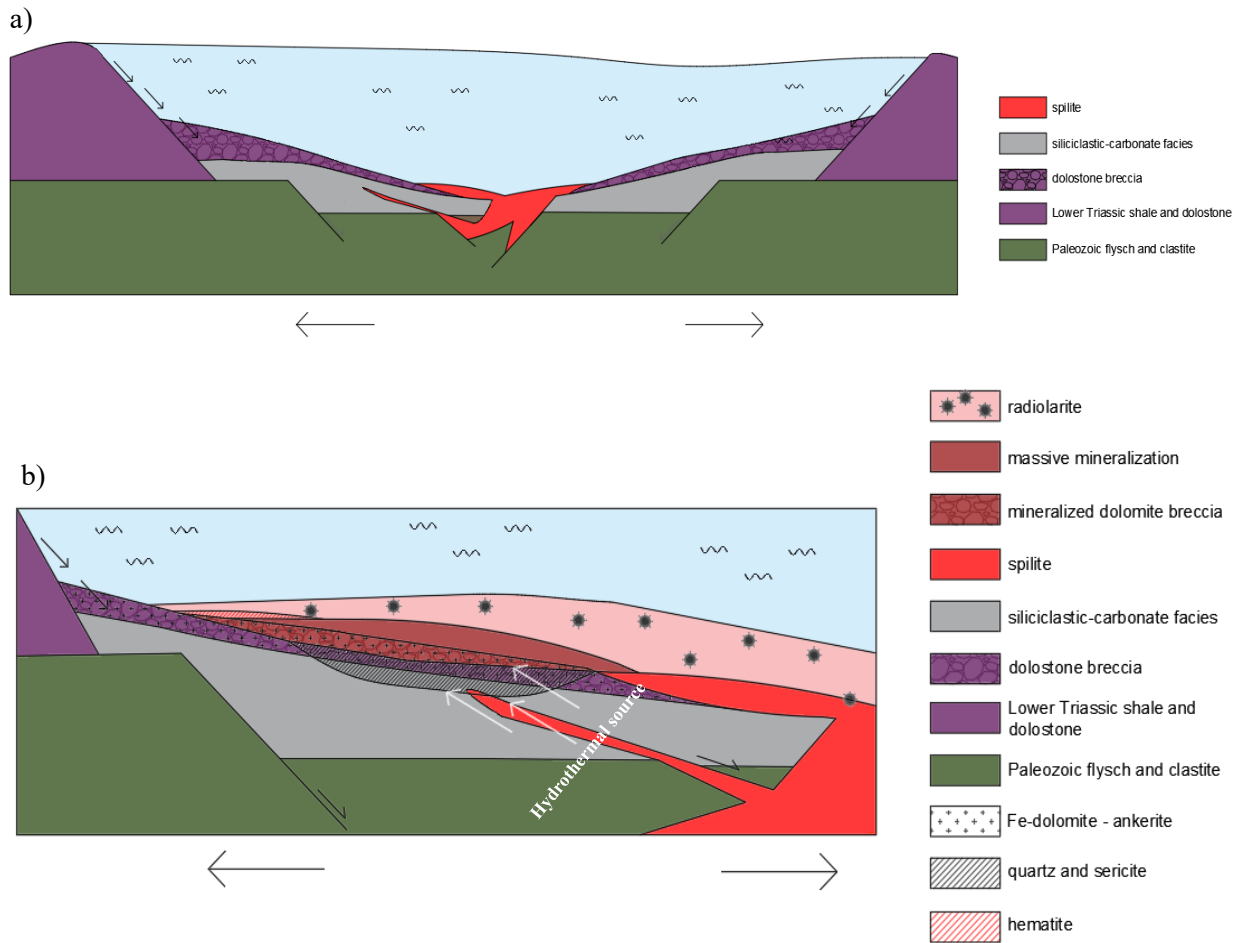


**Figure 0-1.** Anisian opening of the Tethys basin.

### 6.3.2. The second phase: Anisian – Ladinian

During the Anisian-Ladinian period, the basin subsided due to advanced rifting, which led to the tectonic fragmentation of the Lower Triassic and Paleozoic material and the formation of dolomitic breccia (Fig. 6-2. A). Radiolarites, which are stratigraphically younger than the carbonate-silicate facies, were deposited. This phase was associated with the eruption of spilite onto the seafloor, mineralization, and alteration of surrounding rocks related to the ore-bearing stage. The occurrence of radiolarians in tuffs in the footwall and the radiolarites in the hanging wall indicates that mineralization occurred syn-sedimentary with the mentioned phases.

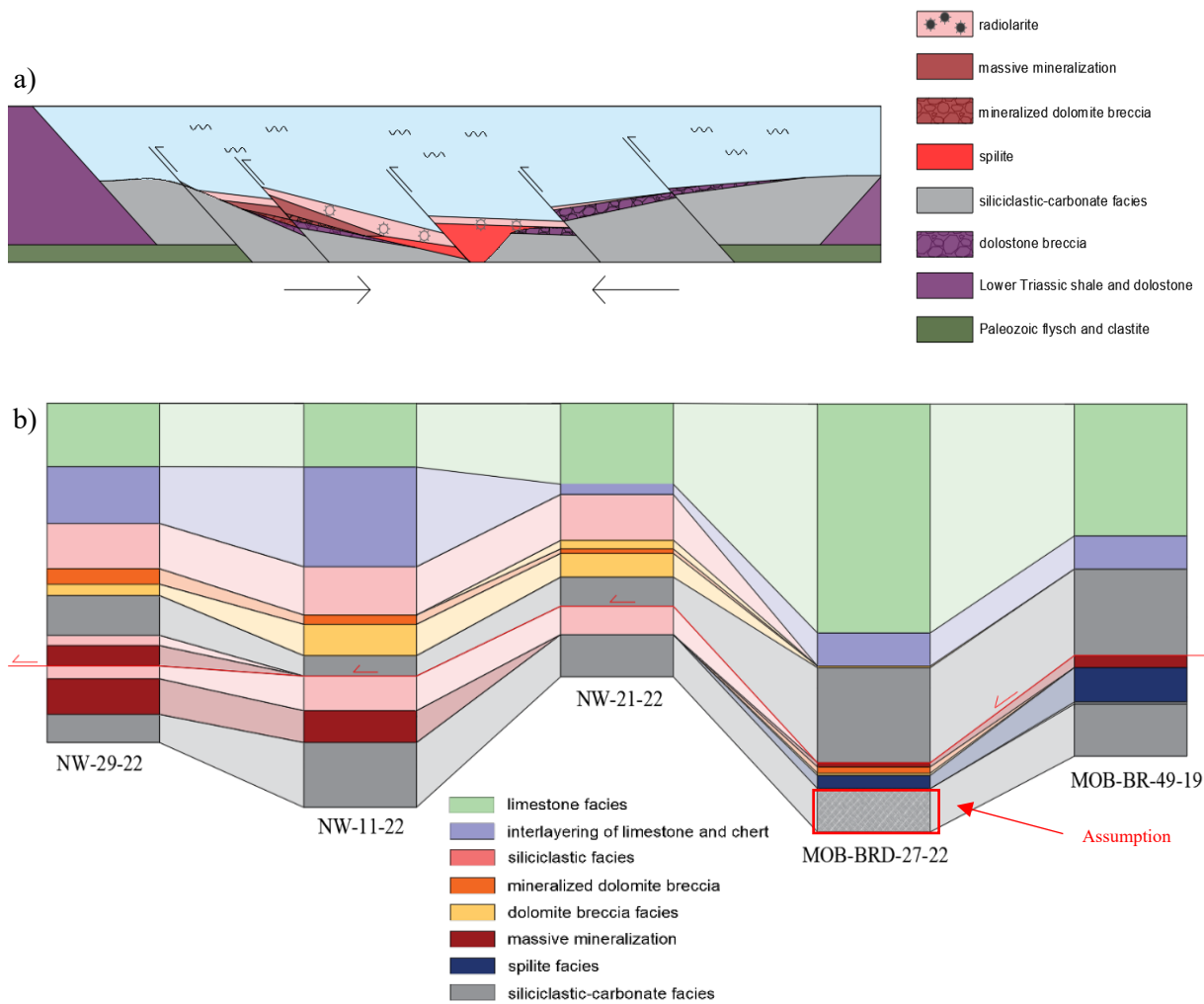
The dolomitic breccia displays a distinct mineralization pattern, beginning with sulphide-rich breccia and progressing from massive sulphide to barite mineralization. Notably, there is no evidence of mineralization in the underlying spilites. These observations suggest that the fluid responsible for the ore's deposition was likely derived from magma and is arranged by the temperature sequence of sulphide and barite mineralization in the upper regions of the formation. The metal zonation is typical for Volcanogenic Massive Sulphide (VMS) ore deposits (G. Gisbert et al., 2021). Linked to a hydrothermal event, the rocks in the footwall were altered into quartz and sericite. Proximal to the hydrothermal source, radiolarian cherts are enriched in silica, while distally radiolarians are hematitized. The Fe-dolomite-ankerite cement was believed to have been created during this hydrothermal phase (Fig. 6-2. B).



**Figure 0-2. A)** Anisian-Ladinian advanced rifting, associated with spilite eruption on the seafloor; **B)** Ore-bearing hydrothermal event and alteration halos.

### 6.3.3. The third phase: Eocene – Oligocene

During the Eocene-Oligocene, the closure of the basin was initiated, resulting in reverse faulting and overthrusting (Fig. 6-3. A). As the pressure and temperature increased, recrystallization occurred along fault planes, potentially leading to the recrystallization of minerals within the deposit and the growth of framboidal pyrite. The sign of reverse faulting is visible in borehole NW-29-22 – as the massive mineralization and radiolarite were reversely faulted on a local scale. With further basin closure, the pressure increased, and deeper rocks were affected by tectonism. Consequently, radiolarite had been overthrust by the footwall's siliciclastic-carbonate host rocks and mineralized dolomitic breccia (Fig. 6-3. B). It is presumed that the Upper zone is situated distally from the feeder zone and the centre of magmatic activity, hence the absence of massive sulphide, barite, and spilite. During the quiescent phase of tectonic activity, limestones were deposited.



**Figure 0-3. A)** Eocene-Oligocene basin closure and reverse faulting; **B)** recent duplex-structure of the deposit.

#### 6.3.4. The fourth phase: recent

In the recent phase, the host rocks have been altered under the influence of weathering. As a result, there is a noticeable hematitization and limonitization of limestone facies.

## 7. CONCLUSION

The Rupice deposit is situated in the central Dinarides, between the Bosnian flysch nappe and the Ophiolite nappe. It contains polymetallic mineralization, such as barite, galena, sphalerite, pyrite, chalcopyrite, and various sulfosalts, with a high content of silver (156 g/t), gold (1.2 g/t), zinc (4.3%), lead (2.8%), copper (0.4%), and BaSO<sub>4</sub> (27%). The deposit structure is duplex, consisting of the Main and the Upper mineralized zones, with the host rock being dolomitic breccia.

The study aimed to investigate the petrology, geochemistry, and mineralogy of the deposit further and determine lithological members and their depositional conditions. Fourteen lithotypes were identified, including dolomitic marl, silicified marl, dolomitic siltstone, silicified siltstone, dolomicrite, LD dolomite, tuff, amygdaloidal basalt, spilite breccia, radiolarite, barite-sulphide mineralization, mineralized dolomitic breccia, dolomitic breccia, and limestone.

Siliciclastic-carbonate, chert, and spilitic facies contain fossil fauna indicating deposition in a deep-sea environment, such as thin-shelled molluscs and radiolarians. The siliciclastic-carbonate unit is the oldest and belongs to the Anisian stage. At the same time, the mineralized zone formed syn-sedimentarily with radiolarites and spilites, and its age can be constrained to the upper Anisian-lower Ladinian stage.

The structure formed due to reverse faulting, with older siliciclastic-carbonate facies overlying younger radiolarites. Supporting evidence includes the double repetition of the stratigraphic sequence- siliciclastic-carbonate rocks, mineralization, and radiolarite within boreholes, as well as the duplication of overthrusts siliciclastic-carbonate facies with the mineralized zone (absence of radiolarite). In the overthrust Upper zone, mineralized breccia, associated with the siliciclastic-carbonate unit, is overlain by pyroclastic material. This supports the fact that spilites erupted onto the oldest unit - siliciclastic-carbonate.

The siliciclastic-carbonate unit was deposited during the opening of the Tethys basin in the Anisian. Radiolarians were deposited as the basin deepened and subsided during the transition from the Anisian to the Ladinian. This phase is associated with a magmatic stage in which spilites erupted on the seafloor and a hydrothermal phase responsible for the mineralization and accompanying alterations of surrounding rocks. Surrounding sedimentary rocks are silicified and sericitized. The deposit exhibits metal zoning from massive sulphides to barite,



suggesting it is a VMS-type deposit. In the Eocene-Oligocene, the basin closed due to reverse faulting, and the structure took on its present appearance. Temperature and pressure changes along fault planes may have caused possible mineral recrystallization and the formation of framboidal pyrite. When tectonic activity subsided, recent mudstone was deposited. Its characteristics indicate different depositional conditions than other rocks, such as the absence of deep-sea fossils, silicification, and dolomitization. The rocks underwent weathering alterations in the recent phase, forming secondary minerals such as hematite, limonite, and clay.

## 8. REFERENCES

- AUSTEN, K.F., WRIGHT, K., SLATER, B. AND GALE, J.D., (2005): *The interaction of dolomite surfaces with metal impurities: a computer simulation study*. Physical Chemistry Chemical Physics, 24(7), str. 4150-4156.
- CELARC, B.; GORIČAN, Š. AND KOLAR-JURKOVŠEK, T. (2013): *Middle Triassic carbonate platform break-up and formation of small-scale half-grabens (Julian and Kamnik-Savinja Alps, Slovenia)*. Facies, 59, 583–610.
- DE WEVER, P.; DUMITRICA, P.; CAULET, J.P.; NIGRINI, C. AND CARIDROIT, M. (2001): *Radiolarians in the sedimentary record*. Gordon and Breach Science Publications, London, 524 p.
- FLÜGEL E. (2004): *Microfacies of Carbonate Rocks: Diagenesis, Porosity, and Dolomitization*.
- GAWLICK, H.-J.; LEIN, R. AND BUCUR, I.I. (2021): *Precursor extension to the final Neo-Tethys break-up: flooding events and their significance for the correlation of shallow-water and deep marine organisms (Anisian, Eastern Alps, Austria)*. International Journal of Earth Sciences, 110, 419–446. <https://doi.org/10.1007/s00531-020-01959-w>.
- GIANOLLA, P.; DE ZANCHE, V. AND MIETTO, P. (1998): *Triassic sequence stratigraphy in the Southern Alps (Northern Italy): definition of sequence and basin evolution*.
- GORIČAN, Š. AND BUSER, S. (1988): *Middle Triassic radiolarians from Slovenia (Yugoslavia)*. Geologija, 31, 133–197.
- HRVATOVIĆ, H. (2006): *Geološki vodič kroz Bosnu i Hercegovinu*.
- JURKOVŠEK, B. AND HRVATOVIĆ, H. (2018): *Stratigraphic definition and correlation of the Middle Triassic volcanoclastic facies in the External Dinarides: Croatia and Bosnia and Herzegovina*. Journal of Earth Sciences, 29, 864–878. <https://doi.org/10.1007/s12583-018-0789-1>
- MCPHIE, J., DOYLE., M., & ALLEN, R. (1993): *Volcanic textures – A guide to the interpretation of textures in volcanic rocks*. Centre for Ore Deposit and Exploration Studies, University of Tasmania, 198 pp.
- PAMIĆ, J. (1984): *Triassic magmatism of the Dinarides in Yugoslavia*.

PAMIĆ, J. et. al (1997): *Alpine magmatic-metallogenic formations of the northwestern and central Dinarides*.

RAJABI, A. (2018): *The role of framboidal pyrite in determining the genesis of sedimentary ore deposits*.

SLOVENEK, D.; ŠEGVIĆ, B.; HALAMIĆ, J.; GORIČAN, Š. AND ZANONI, G. (2020): *An ensialic volcanic arc along the northwestern edge of Palaeotethys-Insights from the Mid-Triassic volcano-sedimentary succession of Ivanščica Mt. (northwestern Croatia)*. Geological Journal, 55, 4324–4351. <https://doi.org/10.1002/gj.3664>

SLOVENEK, D., (2002): *Sistematska mineralogija: interna skripta*. Zagreb: Rudarsko-geološko-naftni fakultet.

SRIVASTAVA, P.K. AND SUKCHAIN, (2005): *Petrographic Characteristics and Alteration Geochemistry Granite-hosted Tungsten Mineralization at Degana, NW India*. Resource Geology, 55(4), str. 373-384.

TRUBELJA, F. (2004): *Triassic Magmatism in the Area of the Central Dinarides (Bosnia and Herzegovina): Geochemical Resolving of Tectonic Setting*.

SMIRČIĆ, D.; KOLAR-JURKOVŠEK, T.; ALJINOVIĆ, D.; BARUDŽIJA, U.; JURKOVŠEK, B. AND HRVATOVIĆ, H. (2018): *Stratigraphic definition and correlation of the Middle Triassic volcanoclastic facies in the External Dinarides: Croatia and Bosnia and Herzegovina*. Journal of Earth Sciences, 29, 864–878. <https://doi.org/10.1007/s12583-018-0789-1>

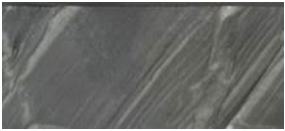
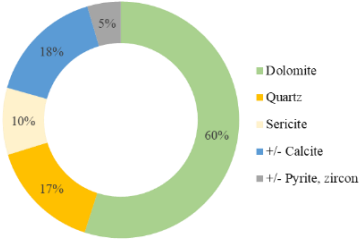

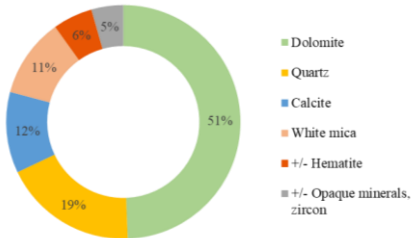
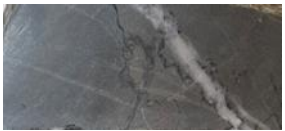
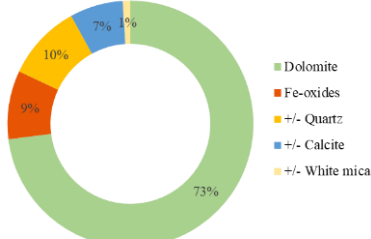
SMIRČIĆ, D.; JAPUNDŽIĆ, D.; GABERŠEK, N.; ALJINOVIĆ, D.; PRLJ-ŠIMIĆ, N.; BORČIĆ, N.; KRIZMANIĆ, K.; PAVIĆ, I. AND BARUDŽIJA, U. (2020): *First record of the upper Illyrian ammonoid subzone marker *Reitziites reitzi* in the Karst Dinarides*. Rudarsko Geološko Naftni Zbornik, 35, 75–84. <https://doi.org/10.17794/rgn.2020.2.7>

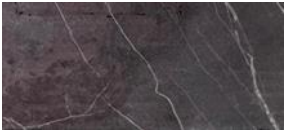
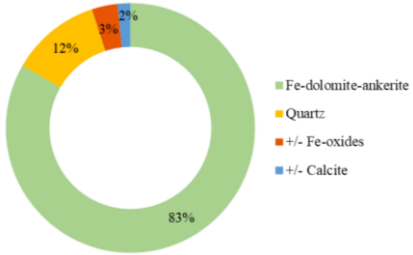

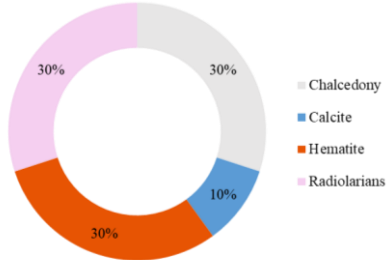

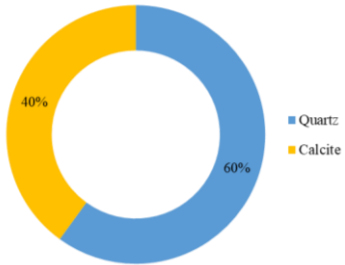

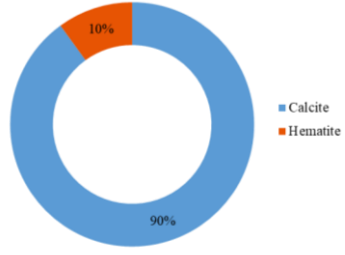
SUDAR, M.; GAWLICK, H.-J.; LEIN, R.; MISSONI, S.; KOVÁCS, S. AND JOVANOVIĆ, D. (2013): *Depositional environment, age and facies of the Middle Triassic Bulog and Rid Formations in the Inner Dinarides (Zlatobor Mountain, SW Serbia): evidence for the Anisian break-up of the Neotethys Ocean*. Neues Jahrbuch für Geologie und Paläontologie Abhandlungen, 269, 291–320. <https://doi.org/10.1127/0077-7749/2013/0352>

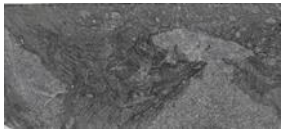
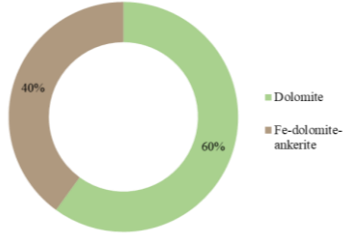

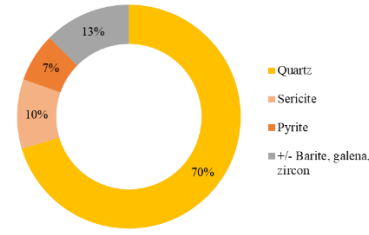

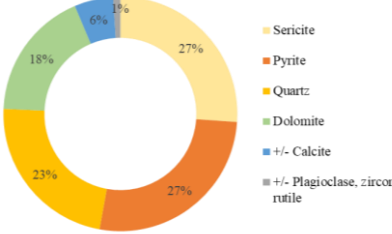

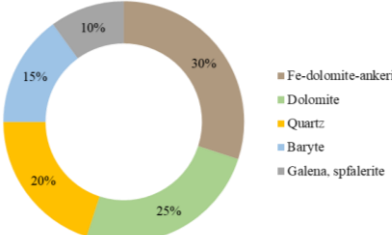
Internet sources:

Geographical position of the study area. URL: <https://earth.google.com/web/>

**Table 8-1.** Catalogue of the lithotypes.

	<i>Lithotypes</i>	<i>Core features</i>	<i>Microscope features</i>	<i>Average mineralogy</i>	<i>Main features</i>	<i>Sedimentary environment and origins</i>	<i>Age determination</i>
<i>Footwall</i>	<i>Dolomitic marl</i>		Rhythmic alteration of dolomitic and sericitic laminae	 <ul style="list-style-type: none"> <li>■ Dolomite</li> <li>■ Quartz</li> <li>■ Sericite</li> <li>■ +/- Calcite</li> <li>■ +/- Pyrite, zircon</li> </ul>	Shaly texture, sub-parallel oriented laminae	Deep marine environment	Anisian
	<i>Dolomitic siltstone</i>		Silty detritic cement interbedded with limestone fragments and sandstone composed of quartz, dolomite, and muscovite cemented with dolomite; oxidized foliation	 <ul style="list-style-type: none"> <li>■ Dolomite</li> <li>■ Quartz</li> <li>■ Calcite</li> <li>■ White mica</li> <li>■ +/- Hematite</li> <li>■ +/- Opaque minerals, zircon</li> </ul>	Shaly texture, thinner laminae than marl and walogite	Deep marine environment	Anisian
	<i>Homogeneous dolomiticrite</i>		Silty, clayey non-ferrous dolomite cemented with quartz and clay minerals	 <ul style="list-style-type: none"> <li>■ Dolomite</li> <li>■ Fe-oxides</li> <li>■ +/- Quartz</li> <li>■ +/- Calcite</li> <li>■ +/- White mica</li> </ul>	Fine-grained dolomite, doesn't react with 10% HCl	Deep marine environment	Anisian

	<i>Massive LD dolostone</i>		Saddle-like coarse Fe-dolomite-ankerite with undulatory extinction, and blue colouration on the carbonate staining test	 <ul style="list-style-type: none"> <li>Fe-dolomite-ankerite</li> <li>Quartz</li> <li>+/- Fe-oxides</li> <li>+/- Calcite</li> </ul>	Coarse-grained Fe-dolomite in contact with ore-bearing and volcanogenic units	Deep marine environment	Anisian
Hanging wall	<i>Hematitized radiolarite</i>		Hematitized chert with calcedony-filled radiolarias	 <ul style="list-style-type: none"> <li>Chaledony</li> <li>Calcite</li> <li>Hematite</li> <li>Radiolarians</li> </ul>	Massive red unit, crosscutted with calcite veins, hardness approximately 7 on the Mohs scale	Deep marine environment	Anisian-Ladinian
	<i>Unaltered radiolarite</i>		Fine-grained chert with radiolarians, thin-shelled molluscs and calcite veins	 <ul style="list-style-type: none"> <li>Quartz</li> <li>Calcite</li> </ul>	Massive gray (unaltered) or red (hematitization) unit crosscutted with calcite tensional veins, hardness approximately 7 on the Mohs scale	Deep marine environment	Anisian-Ladinian
	<i>Mudstone</i>		Fine-grained calcite mudstone partially embedded with limestone fragments	 <ul style="list-style-type: none"> <li>Calcite</li> <li>Hematite</li> </ul>	Calcite reacts rapidly and easily with 10% HCl; embedded pale limestone fragments in laminated texture	Shallow marine environment	?Jurassic

Magmatic-hydrothermal event	<i>Unmineralized dolomitic breccia</i>		Dolostone fragments with Fe-dolomite-ankerite matrix	 <ul style="list-style-type: none"> <li>■ Dolomite</li> <li>■ Fe-dolomite-ankerite</li> </ul>	Light gray, unsorted, angular dolostone fragments within dark gray, Fe-dolomite-ankerite matrix	Deep marine environment	Anisian-Ladinian
	<i>Silicified marl</i>		Interlayering of quartz-pyritic and white micaceous laminae	 <ul style="list-style-type: none"> <li>■ Quartz</li> <li>■ Sericite</li> <li>■ Pyrite</li> <li>■ +/- Barite, galena, zircon</li> </ul>	Interlayering of pale red and gray laminae, doesn't react with 10% HCl, with hardness ranging from 6-7 on the Mohs scale	Deep marine environment	Anisian-Ladinian
	<i>Silicified siltstone</i>		Rhythmic alteration of foliated quartz-pyrite and sericite laminae; pyritized limestone fragments	 <ul style="list-style-type: none"> <li>■ Sericite</li> <li>■ Pyrite</li> <li>■ Quartz</li> <li>■ +/- Calcite</li> <li>■ +/- Plagioclase, zircon, rutile</li> <li>■ +/- Barite, galena, zircon</li> </ul>	Shaly texture, rhythmic alteration of foliated darker, quartz-pyritic laminae and lighter, sericitic laminae	Deep marine environment	Anisian-Ladinian
	<i>Mineralized dolomitic breccia</i>		Dolostone fragments with mineralized ferrous dolomite-ankerite matrix (+/-barite, pyrite, galena, sphalerite)	 <ul style="list-style-type: none"> <li>■ Fe-dolomite-ankerite</li> <li>■ Dolomite</li> <li>■ Quartz</li> <li>■ Baryte</li> <li>■ Galena, sphalerite</li> </ul>	Angular, unsorted dolostone fragments within ore bearing matrix	Deep marine environment	Anisian-Ladinian

<p><i>Massive mineralization</i></p>		<p>At least two generations of barite; 1. massive, idiomorphic grains, 2. vein-filling barite</p>	 <ul style="list-style-type: none"> <li>■ Barite</li> <li>■ +/- Pyrite, marcasite, sphalerite, galena, tetrahedrite</li> </ul>	<p>Metal zonation from massive sulphide (galena, sphalerite, pyrite) to massive barite</p>	<p>Deep marine environment</p>	<p>Anisian-Ladinian</p>
<p><i>Homogenous to laminated tuff</i></p>		<p>Fine-grained quartz, volcanic glass fragments (V- and Y-shaped), and radiolarians in „flowy“ structure</p>	 <ul style="list-style-type: none"> <li>■ Quartz</li> <li>■ Chlorite</li> <li>■ Volcanic glass</li> <li>■ Plagioclase</li> <li>■ Clay minerals</li> <li>■ Calcite</li> <li>■ Biotite</li> </ul>	<p>Dark green, compact tuff with visible layering and friable, pale green varieties with a shale texture</p>	<p>Deep marine environment</p>	<p>Anisian-Ladinian</p>
<p><i>Brecciated spilite</i></p>		<p>Sharp and irregular-edged spilitic fragments secondary cemented with calcite</p>	 <ul style="list-style-type: none"> <li>■ Plagioclase</li> <li>■ Hematite</li> <li>■ Matrix</li> <li>■ Calcite</li> <li>■ Chlorite</li> </ul>	<p>Brown to purple, sharp-edged spilitic fragments with calcite- and rhodochrosite-filled voids</p>	<p>Deep marine environment</p>	<p>Anisian-Ladinian</p>
<p><i>Amygdaloidal basalt</i></p>		<p>Regular and rounded amygdalas filled with calcite, celadonite, and chlorite</p>	 <ul style="list-style-type: none"> <li>■ Plagioclase</li> <li>■ Matrix</li> <li>■ Calcite</li> <li>■ Chlorite</li> <li>■ Celadonite</li> <li>■ +/- Hematite</li> </ul>	<p>Pale to dark green amygdaloidal basalt with calcite-, celadonite and chlorite-filled vesicle</p>	<p>Deep marine environment</p>	<p>Anisian-Ladinian</p>

